HHS Public Access

Author manuscript

Cell. Author manuscript; available in PMC 2018 April 06.

Published in final edited form as:

Cell. 2017 April 06; 169(2): 258–272.e17. doi:10.1016/j.cell.2017.03.023.

Physiologic medium rewires cellular metabolism and reveals uric acid as an endogenous inhibitor of UMP synthase

Jason R. Cantor[1,2,3,4], **Monther Abu-Remaileh**[1,2,3,4], **Naama Kanarek**[1,2,3,4], **Elizaveta Freinkman**[1], **Xin Gao**[1,5], **Abner Louissaint Jr.**[6], **Caroline A. Lewis**[1], and **David M. Sabatini**[1,2,3,4]

[1]Whitehead Institute for Biomedical Research and Massachusetts Institute of Technology, Department of Biology, 9 Cambridge Center, Cambridge, MA 02142, USA

[2]Howard Hughes Medical Institute, Department of Biology, Massachusetts Institute of Technology, Cambridge, MA 02139, USA

[3]Koch Institute for Integrative Cancer Research, 77 Massachusetts Avenue, Cambridge, MA 02139, USA

[4]Broad Institute of Harvard and Massachusetts Institute of Technology, 7 Cambridge Center, Cambridge, MA 02142, USA

[5]Beth Israel Deaconess Medical Center, Department of Medicine, Harvard Medical School, 330 Brookline Avenue, Boston, MA 02215

[6]Massachusetts General Hospital, Department of Pathology, 55 Fruit Street, Boston, MA 02114

SUMMARY

A complex interplay of environmental factors impacts the metabolism of human cells, but neither traditional culture media nor mouse plasma mimic the metabolite composition of human plasma. Here, we developed a culture medium with polar metabolite concentrations comparable to those of human plasma (human plasma-like medium; HPLM). Culture in HPLM, relative to that in traditional media, had widespread effects on cellular metabolism, including on the metabolome, redox state, and glucose utilization. Among the most prominent is an inhibition of de novo pyrimidine synthesis – an effect traced to uric acid, which is 10-fold higher in the blood of humans than of mice and other non-primates. We find that uric acid directly inhibits UMP synthase and

Correspondence should be addressed to D.M.S., Tel: 617-258-6407; Fax: 617-452-3566; sabatini@wi.mit.edu.

Lead contact: David M. Sabatini

SUPPLEMENTAL INFORMATION

Supplemental information includes all methods, seven figures, and four tables.

AUTHOR CONTRIBUTIONS

J.R.C. and D.M.S. initiated the project and designed the research. J.R.C. performed the experiments and analyzed the data with input from M.A.-R., N.K., and E.F. M.A.-R. also assisted with plasma isolation. N.K. also assisted in drug treatment and transduction experiments. E.F. also assisted in the design of LC/MS methods. X.G. assisted with plasma isolation. A.L. collected the primary AML specimen. C.A.L. and E.F. operated the LC/MS equipment. J.R.C. and D.M.S. wrote and edited the manuscript.

consequently reduces the sensitivity of cancer cells to the chemotherapeutic agent 5-fluorouracil. Thus, media that better recapitulates the composition of human plasma reveals unforeseen metabolic wiring and regulation, suggesting that HPLM should be of broad utility.

Graphical abstract

Mimicking the metabolite composition of human plasma in culture reveals new tumor specific liabilities and metabolite-drug interactions

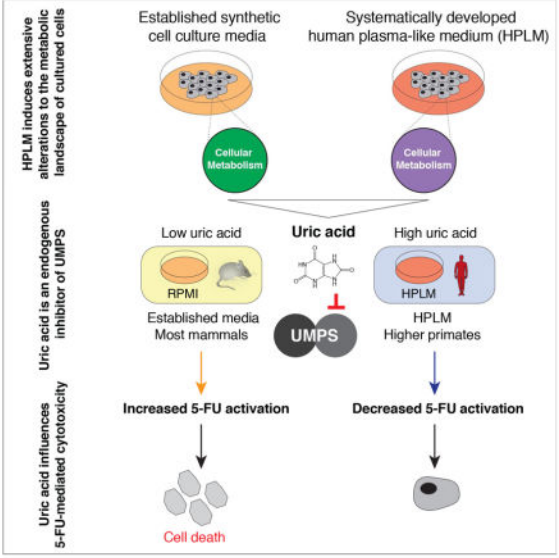

INTRODUCTION

There is a resurgence of interest in the metabolism of mammalian cells and in understanding the metabolic adaptations that enable cells to grow and proliferate (DeBerardinis et al., 2008; Hosios et al., 2016; Keibler et al., 2016; Lunt and Vander Heiden, 2011; MacIver et al., 2013; Pearce et al., 2013; Vander Heiden et al., 2009). Cells in culture are commonly used to study metabolism (DeBerardinis and Chandel, 2016) and despite the appreciation that metabolic networks are flexible (Boroughs and DeBerardinis, 2015; Cairns et al., 2011; Cantor and Sabatini, 2012; Lehuede et al., 2016; Olson et al., 2016) and greatly influenced by environmental metabolites (Davidson et al., 2016; DeBerardinis and Chandel, 2016; DeNicola and Cantley, 2015; Hensley et al., 2016; Maddocks et al., 2013; Mayers et al., 2016; Yuneva et al., 2012), there has been relatively little investigation of how the small molecule composition of culture media impacts metabolism.

Traditional synthetic cell culture media were not developed with the primary desire of mimicking human plasma, but, rather, to address the need for large amounts of medium with less inherent variability than natural media such as biological fluids and tissue extracts (Freshney, 2010). Upon defining the minimum nutritional requirements of two cell types (Eagle, 1955a; 1955b), Eagle formulated one of the first standardized synthetic media, Basal Medium Eagle (BME), over half a century ago (Eagle, 1955c). Soon after, Eagle developed

Minimal Essential Medium (MEM) (Eagle, 1959), and within the ensuing decade, Dulbecco and Freeman formulated DMEM (Dulbecco's Modified Eagle Medium) originally for the culture of mouse embryonic cells (Dulbecco and Freeman, 1959), and Moore and colleagues developed RPMI 1640 for that of blood cells (Moore et al., 1967). Even though the nutrient concentrations of DMEM and RPMI 1640 poorly resemble those of human plasma, most studies of metabolism examine cells cultured in these media.

Efforts have been made to adjust the concentrations of media components, usually one or several nutrients at a time, to better reflect physiologic conditions (Birsoy et al., 2014; Favaro et al., 2012; Kamphorst et al., 2015; Pan et al., 2016; Schug et al., 2015; Tardito et al., 2015; Yao et al., 2016). Most such modified media not only contain other nutrients at non-physiological levels, but also lack defined concentrations of many metabolites now known to be present in human plasma. In mice and humans, great progress has been made in the study of metabolism *in vivo*, usually by monitoring the utilization patterns of isotope-labeled nutrients in tumors or normal tissues (Comerford et al., 2014; Commisso et al., 2013; Davidson et al., 2016; Hensley et al., 2016; Mashimo et al., 2014; Mayers et al., 2016; Sellers et al., 2015; Venneti et al., 2015; Yuneva et al., 2012). While such models provide a physiologically relevant environmental context for the study of metabolism, they do not permit the scope and flexibility of experimentation possible in cultured cells. In addition, there are multiple examples of differences in the metabolism of mice and humans (Adelman et al., 1988; Chandrasekera and Pippin, 2014; Demetrius, 2005; Elsea and Lucas, 2002; Martignoni et al., 2006), and it is unclear how well the metabolite composition of murine plasma reflects that of humans.

Here, we developed a medium with a defined set of metabolites and salts at the concentrations reported for adult human plasma (human plasma-like medium; HPLM). Culture in HPLM dramatically alters the metabolism of cells compared to that in traditional media. Among its most prominent effects is an inhibition of de novo pyrimidine synthesis, which we traced to uric acid – a metabolite whose plasma concentration is up to an order of magnitude greater in higher primates than in other mammals (Álvarez-Lario and Macarrón-Vicente, 2010; Kratzer et al., 2014; Wu et al., 1992). We find that uric acid directly inhibits UMP synthase (UMPS), and consequently, reduces the sensitivity of cancer cells to the chemotherapeutic agent 5-fluorouracil. While we traced the effects of HPLM on pyrimidine metabolism to uric acid, the causes for most of the metabolic effects we observe are unknown and of potential interest for future study.

RESULTS AND DISCUSSION

A cell culture medium that reflects the polar metabolite composition of human plasma

The classic synthetic cell culture media, BME, MEM, DMEM, and RPMI 1640, contain glucose, amino acids, vitamins, and salts at concentrations that in large part do not reflect those of human plasma (Figure 1A, Table S1). These media also lack additional components revealed to be present by mass spectrometric and NMR analyses of plasma (Psychogios et al., 2011). Instead, basal media are often supplemented with heat inactivated fetal bovine serum (IFS), which contributes an undefined and often unaccounted for cocktail of metabolites, as well as the growth factors and hormones needed for cell proliferation

(Freshney, 2010). Thus, while the impact of environmental factors on cell metabolism is well appreciated (Davidson et al., 2016; DeNicola and Cantley, 2015; Hensley et al., 2016; Maddocks et al., 2013; Mayers et al., 2016; Yuneva et al., 2012), the interrogation of cultured cells in media that better reflect the metabolite composition of human plasma is largely unexplored (Figure 1B).

To begin to address this, we developed a culture medium with a defined collection of metabolites and salt ions at concentrations reported for plasma from healthy adult humans (human plasma-like medium; HPLM) (Psychogios et al., 2011; Wishart et al., 2013). Although some serum-free media have entirely defined recipes, they often require meticulous tailoring of growth factors to support the culture of different cell types (Freshney, 2010). Thus, given our hope that HPLM will be of broad utility, we supplemented it with 10% dialyzed IFS ($HPLM^{+dIFS}$) to add the growth factors and hormones required for the proliferation of a broad range of cells, while minimizing the addition of polar metabolites at unknown concentrations. We did not attempt to recapitulate the lipophilic components of human serum because the removal of serum lipids present at otherwise unknown concentrations requires a charcoal stripping step that can deplete certain hormones and growth factors. As anticipated, dialyzed IFS contains total, LDL, and HDL cholesterol at concentrations equivalent to those in IFS (Table S1). The Supplemental Experimental Methods describes $HPLM^{+dIFS}$ in detail, but, in brief, it contains glucose, proteinogenic amino acids, salts, twenty-seven additional polar metabolites, 10% dialyzed IFS and vitamins at the same concentrations as RPMI 1640 (Figure 1C, Table S1); uses a bicarbonate buffering system at physiological pH; and has an osmolality of ~295 mOsm/kg.

Because RPMI 1640 (herein RPMI) is the medium of choice for culturing normal blood cells as well as the hematological cancer cells we examine in detail below (Freshney, 2010; Moore et al., 1967), we chose it as the reference medium for comparing the effects of $HPLM^{+dIFS}$ on cells. We generated two RPMI formulations, each with physiological glucose (5 mM), but supplemented with either 10% IFS ($RPMI^{+IFS}$) or 10% dialyzed IFS ($RPMI^{+dIFS}$). Metabolite profiling confirmed that the dialysis of IFS substantially reduced its levels of polar metabolites, but had little effect on its lipid contents (Figure 1D, Table S1). Moreover, it also revealed that fetal bovine serum poorly reflects the metabolic composition of adult human plasma, as the addition of 10% IFS to RPMI did not yield concentrations for many metabolites at 10% of the reported values in human plasma. Similarly, while the concentrations of glucose and many amino acids in mouse plasma in large part resemble those in human plasma, those of other metabolites were very different, including examples that were at least 3–10-fold lower (e.g. carnitine and uric acid) or greater (e.g. 3-hydroxybutyrate and taurine) in mouse plasma (Figure 1D, Table S1). Thus, while murine tumor models are useful for studying metabolism in the context of stromal and immune cells, $HPLM^{+dIFS}$ more closely reflects the polar metabolite composition of human plasma than does mouse plasma.

$HPLM^{+dIFS}$ provides the metabolites needed for cancer cell proliferation, as six cell lines representing various human hematological cancers as well as four cell lines from diverse human epithelial cancers proliferated in $HPLM^{+dIFS}$ at rates that were comparable, albeit generally lower, to those in $RPMI^{+IFS}$ and $RPMI^{+dIFS}$ (Figure 1E, Figure S1A). $HPLM^{+dIFS}$

also supports efficient viral-based transduction (Figure S1B), and cells cultured in HPLM^{+dIFS} activated mTORC1 signaling to an extent comparable to those in RPMI^{+IFS}, as detected by phosphorylated S6K1 (Figure S1C).

Culture of cells in HPLM extensively alters their metabolic landscape and fate of glucose carbons

To test the hypothesis that culturing cells in a medium that better mimics the metabolic composition of human plasma alters cellular metabolism compared to that in established media, we began by comparing the metabolite profiles of cells cultured in HPLM^{+dIFS} to those in RPMI^{+IFS} or RPMI^{+dIFS}. Indeed, HPLM^{+dIFS} profoundly affected the intracellular abundances of many metabolites across multiple pathways, including amino acid, lipid, and nucleotide metabolism (Figure 2A, Table S2). For several metabolites, such as arginine, asparagine, and taurine, the differences reflected those in the media themselves, while for others, such as aspartate and lactate, they did not. Most HPLM^{+dIFS}-induced changes were shared by all six of the cell lines examined, but some were cell line-specific, underscoring how the heterogeneity of cancer (Cantor and Sabatini, 2012; Eason and Sadanandam, 2016; Hu et al., 2013; Shaul et al., 2016) can influence the cellular responses to environmental conditions. For example, whereas HPLM^{+dIFS} reduced argininosuccinate abundance in five cell lines, it increased it in P12-Ichikawa cells. Similarly, HPLM^{+dIFS} caused dramatic elevations in fructose-6-phosphate/glucose-1-phosphate (F6P/G1P) only in K562, P12-Ichikawa, and SUDHL4 cells, and modest reductions in oxoglutarate only in KMS12BM cells. Culture in HPLM^{+dIFS} also induced widespread and largely similar alterations to the metabolomes of several other cell types, including a variety of epithelial cancer cell lines (786-0, A549, MCF7, and SW620), an early passage undifferentiated sarcoma cell line (CLF-PED-015T (Hong et al., 2016)), a normal foreskin fibroblast cell line (BJ), and a primary acute myeloid leukemia sample (Figure S2A, Table S3).

Culture in HPLM^{+dIFS} did not affect the energy charge (Atkinson, 1968) in any cell line (Figure 2B), but did have cell line-specific effects on the redox state as reflected by changes to the ratios of two redox couples: GSH/GSSG (Figure 2C) and NAD/NADH (Figure 2D). HPLM^{+dIFS} did not markedly alter the correlation between rates of glucose consumption and lactate secretion across four cell lines examined (Figure S2B), suggesting that it had little effect on the aerobic glycolysis phenotype common to most cancer cells (Hosios et al., 2016; Jain et al., 2012). In contrast, HPLM^{+dIFS} reduced basal oxygen consumption rates in two of the same four cell lines, revealing a cell line-specific impact on mitochondrial respiration (Figure S2C). Lastly, the levels of defined components in HPLM^{+dIFS} and RPMI^{+IFS} were largely unaffected following the culture of three cell lines in conditions identical to those used to obtain whole-cell metabolite profiles (Figure S2D, Table S3).

To specifically study glucose utilization, we compared the ^{13}C-labeling patterns for several metabolites following the culture of three cell lines (K562, NOMO1, and P12-Ichikawa) in HPLM^{+dIFS} containing [U-^{13}C]-glucose to those in RPMI^{+IFS} or RPMI^{+dIFS} (Figure 3A, Table S2). Interestingly, while HPLM^{+dIFS} contains pyruvate at a concentration of ~40 μM, which is over 10-fold greater than that of RPMI^{+IFS}, it did not affect the fraction of pyruvate labeled with three ^{13}C (M3) (Figure 3B). However, HPLM^{+dIFS} did affect the metabolism of

glucose-derived Acetyl-CoA generated by the oxidation of pyruvate, as reflected by reductions in the M2 labeling of citrate in the TCA cycle and of certain acetylated amino acids (Figure 3C, Table S2). HPLM^{+dIFS} also decreased the fraction of M3-glycerophosphocholine, suggesting that it may induce alterations in glucose utilization for lipid synthesis (Figure 3D).

As with the metabolome, HPLM^{+dIFS} also had cell-line dependent effects on glucose utilization. Among the most prominent was a dramatic reduction in the M6 labeling of F6P/G1P only in K562 and P12-Ichikawa cells (Figure 3E), suggesting that sources beyond exogenous glucose contribute to F6P/G1P pools when these cells are cultured in HPLM^{+dIFS}. Additionally, while HPLM^{+dIFS} contains alanine at ~620 μM, a concentration nearly 5-fold greater than that of RPMI^{+IFS}, it did not affect the fraction of M3-alanine in two cell lines. However, it reduced by over 2-fold the M3 labeling of alanine in P12-Ichikawa cells (Figure 3F), revealing that HPLM^{+dIFS} impacts the fate of glucose-derived pyruvate in these cells. Nearly all these changes were also observed when comparing cells cultured in HPLM^{+dIFS} to those in RPMI^{+dIFS}, though greater discrepancies in the levels of certain exogenous metabolites, such as pyruvate and alanine, influenced their corresponding ^{13}C labeling patterns (Figure S3A–E, Table S2).

To examine one aspect of cellular nitrogen metabolism, we compared the ^{15}N-labeling patterns for several amino acids following culture of the same three cell lines in HPLM^{+dIFS} containing [α-^{15}N]-glutamine to those in RPMI^{+IFS} or RPMI^{+dIFS} (Figure 3G, Table S2). Interestingly, large differences in amino acid concentrations between HPLM^{+dIFS} and RPMI^{+IFS} influenced corresponding ^{15}N labeling patterns in a cell line-dependent manner. For example, while HPLM^{+dIFS} contains a higher alanine concentration than RPMI^{+IFS}, it reduced the fraction of alanine labeled with one ^{15}N (M1), but only in NOMO1 and P12-Ichikawa cells (Figure 3H). Similarly, though HPLM^{+dIFS} contains asparagine at a concentration of 50 μM, which is nearly 7-fold less than that of RPMI, it dramatically increased the fraction of M1-asparagine, but only in K562 and NOMO1 cells (Figure 3I). In addition, despite containing valine at a concentration roughly equivalent to that of RPMI, HPLM^{+dIFS} nonetheless increased the fraction of M1-valine, but only in K562 and P12-Ichikawa cells (Figure 3J), suggesting it affects the transaminase-mediated transfer of α-^{15}N from glutamine to various amino acids in a cell line-dependent manner. Nearly all these changes were also observed when comparing cells cultured in HPLM^{+dIFS} to those in RPMI^{+dIFS}, though a greater discrepancy in the level of exogenous alanine influenced its corresponding ^{15}N labeling pattern (Figure S3F–H, Table S2).

Collectively, these data reveal that while aerobic glycolysis was essentially unaffected, culture in HPLM^{+dIFS}, compared to that in RPMI, had widespread effects on the metabolic landscape of cells. These include alterations to the metabolome, redox state, mitochondrial respiration, glucose utilization, and nitrogen metabolism, and were either common to all cell lines tested or were cell line-specific. While the causes for many of the changes are unexplained, they do reveal the profound impact of media composition on cellular metabolism.

The uric acid component of HPLM has striking effects on de novo pyrimidine biosynthesis

Among the most dramatic consequences of culture in HPLM^{+dIFS} compared to that in RPMI, were increases in the intracellular abundances of four metabolites involved in nucleotide metabolism: carbamoylaspartate, dihydroorotate, orotate, and orotidine (Figure 4A–D). As none of the four could be detected in either medium, the cause of these changes was not immediately apparent. The first three are intermediates in the de novo pyrimidine biosynthesis pathway that generates UMP, while orotidine is the dephosphorylation product of OMP, which is the immediate precursor to UMP in this pathway (Figure 4E). In four of the six cell lines examined, culture in HPLM^{+dIFS} also reduced by 40–60% the intracellular levels of the UTP and CTP pyrimidine nucleotides (Figure 4F–G), but did not have similar effects on purine nucleotides (Figure S4). Cell line-dependent contributions of salvage pathway activities (Evans and Guy, 2004) or altered consumption of pyrimidine nucleotide pools may explain why HPLM^{+dIFS} does not decrease the abundance of pyrimidine nucleotides in all cells.

To determine which component(s) of HPLM^{+dIFS} affects the de novo pyrimidine synthesis pathway, we cultured K562 cells in HPLM^{+dIFS} derivatives lacking: (1) acetone, creatine, creatinine, formate, fructose, galactose, glutathione, glycerol, and hypoxanthine; (2) non-proteinogenic amino acids (8 metabolites); (3) water-soluble acids (8 metabolites); (4) urea; or (5) uric acid (Figure 5A). Remarkably, uric acid alone mediated the observed effects, as its removal from HPLM^{+dIFS} reduced orotate and orotidine levels to those of cells cultured in RPMI (Figure 3C–D) or in minimal HPLM, which lacks the twenty-seven components collectively missing from the dropout formulations (Figure 5B). HPLM^{+dIFS} contains uric acid at 350 μM, a concentration that is 40- and at least 500-fold greater than that of RPMI^{+IFS} and RPMI^{+dIFS}, respectively (Figure 5C), and, importantly, its intracellular concentration reflects that of the corresponding culture medium (Figure 5D). In K562 cells, uric acid dose-dependently increased orotate and orotidine abundances (Figure 5E), and at its highest tested concentration (700 μM), led to a detectable accumulation of OMP. The addition of 350 μM uric acid to RPMI^{+IFS} also greatly boosted orotate and orotidine levels, but, like complete HPLM, had cell line-dependent effects on UTP abundance (Figure 5F). Lastly, the closely related molecule 9-methyluric acid (9-MUA) entered K562 cells (Table S2), but did not alter the levels of orotate, orotidine, or the other intermediates in the de novo pyrimidine biosynthesis pathway (Figure 5G).

The effects of uric acid on pyrimidine metabolism are particularly interesting because its plasma concentrations are up to an order of magnitude greater in humans, chimpanzees, gorillas, and additional higher primates than in other mammals (Álvarez-Lario and Macarrón-Vicente, 2010; Kratzer et al., 2014; Wu et al., 1992). Whereas most mammalian species, including mouse and cow, metabolize uric acid to allantoin via the liver enzyme uricase, the gene encoding uricase (*UOX*) became inactivated via pseudogenization during hominid evolution (Kratzer et al., 2014; Oda et al., 2002; Wu et al., 1992; 1989). As a consequence, uric acid, rather than allantoin, is the end product of purine catabolism in many higher primates (Figure 5H). Furthermore, in mice, which have a plasma uric acid concentration of ~30 μM, uricase activity is essential, given that most *UOX*-null mice die within four weeks of life from extreme hyperuricemia and nephropathy (Wu et al., 1994).

Thus, the finding that uric acid impacts the de novo pyrimidine biosynthesis pathway would have been difficult to make by studying cells growing in mice or cultured in conventional media.

Uric acid is a direct inhibitor of UMPS

In addition to boosting the intracellular levels of orotate and orotidine, HPLM also markedly increased their secretion into the media (Figure S5A–B) – a phenomenon reminiscent of the high urinary excretion of these metabolites in patients with orotic aciduria and orotidinuria. As this disorder can be caused by the genetic (Bailey, 2009; Fox et al., 1973; Smith et al., 1961; Suchi et al., 1997) or pharmacological (Bono et al., 1964; Fallon et al., 1961; Fox et al., 1970; Kelley and Beardmore, 1970) inhibition of UMP synthase (UMPS), we considered the possibility that the uric acid component of HPLM leads to the inhibition of this enzyme in cells. UMPS is a bifunctional two-domain enzyme that catalyzes the final two steps of the de novo pyrimidine biosynthesis pathway to generate UMP (Jones, 1980). In the first step, the orotate phosphoribosyltransferase (OPRT) domain synthesizes OMP from orotate and PRPP, and in the second, the OMP decarboxylase (ODC) domain converts OMP to UMP (Figure 6A).

To pursue the idea that uric acid might cause inhibition of UMPS, we first asked if an established UMPS inhibitor had similar effects on the de novo pyrimidine biosynthesis pathway as uric acid in our cells. The small molecules allopurinol and 6-azauridine are prodrugs that, upon conversion into allopurinol ribonucleotide and 6-aza-UMP (Bono et al., 1964; Handschumacher, 1960; Kelley and Beardmore, 1970; Murrell and Rapeport, 1986), respectively, competitively inhibit the ODC domain of UMPS (Figure 6B). Indeed, in K562 cells, allopurinol dose-dependently increased the levels of carbamoylaspartate, dihydroorotate, orotate, orotidine, and OMP (Figure S6A–B). Moreover, at its highest tested concentration, allopurinol also decreased by nearly 30% the abundance of UTP in these cells (Figure S6C). Using LC/MS-based metabolite profiling, we detected a species whose mass-to-charge ratio *(m/z)* matched the predicted *m/z* of allopurinol ribonucleotide, and whose magnitude correlated with the concentration of allopurinol in the media (Figure S6D). Importantly, this species could be distinguished from its isomer, IMP, by their differing chromatographic retention times. These data are consistent with the conversion of allopurinol to allopurinol ribonucleotide within the cell. However, despite substantial efforts, we failed to detect in cells a metabolite peak consistent with a putative uric acid ribonucleotide. Thus, we considered if uric acid itself might directly inhibit UMPS.

To investigate this possibility, we developed an in vitro UMPS activity assay containing recombinant UMPS (Figure S6E) and its substrates, orotate and PRPP, and verified its activity via the LC/MS detection of OMP and UMP (Figure 6C). A UMPS mutant (Y37A, R155A), which was designed based on a recently deposited structure of the OPRT domain of human UMPS (Protein Data Bank entry 2WNS, chains A and B) (Figure S6F), had no activity and served as a negative control in the assay. As anticipated, the established ODC inhibitor, 6-aza-UMP, dose-dependently decreased UMP production by UMPS, and at 50 μM, reduced UMP levels to ~3% of those in reactions containing vehicle (Figure 6D). 6-aza-UMP also dramatically increased the abundance of OMP, but the boost in OMP did not

tightly correlate with the decrease in UMP, perhaps owing to the known reversibility of the OPRT reaction (Traut and Jones, 1977).

Remarkably, uric acid also dose-dependently inhibited UMP production by UMPS, and, like 6-aza-UMP, also increased OMP in a fashion that did not completely correlate with the decrease in UMP (Figure 6E). Uric acid was far less potent than 6-aza-UMP, as at 1 mM, it could only reduce UMP levels to ~30% of those in reactions containing vehicle. Importantly, however, uric acid inhibited UMPS in vitro at concentrations consistent with those that boosted orotate and orotidine levels in cultured cells. Lastly, allopurinol and 6-azauridine did not directly inhibit UMPS, and neither did 9-MUA or allantoin (Figure 6F).

Thus, we conclude that uric acid, at the concentrations present in human plasma, is a direct inhibitor of the ODC domain of UMPS.

Uric acid antagonizes the cytotoxicity of 5-fluorouracil

5-fluorouracil (5-FU) is an antimetabolite drug that, although developed over fifty years ago, remains widely used in the treatment of several types of cancer (Longley et al., 2003). In cells, 5-FU is metabolized into various fluoronucleotide derivatives that mediate its cytotoxic effects (Figure 7A). Among these is fluorouridine triphosphate (FUTP), which leads to cell death upon its misincorporation into RNA. FUTP synthesis begins with the conversion of 5-FU to fluorouridine monophosphate (FUMP), either directly by the OPRT domain of UMPS or indirectly through the sequential activities of uridine phosphorylase and uridine kinase (Longley et al., 2003). Previous kinetic studies show that orotate competes with 5-FU for its direct conversion to FUMP by OPRT activity (Reyes and Guganig, 1975) (Figure 7B). Consistent with these findings, allopurinol reduces the sensitivity of certain cancer cell lines to 5-FU (Schwartz and Handschumacher, 1979), owing to orotate accumulation induced by competitive inhibition of the ODC domain of UMPS mediated by allopurinol ribonucleotide. Thus, we reasoned that uric acid might impact the sensitivity of cells to 5-FU through a similar mechanism.

Indeed, culture of NOMO1 cells in $HPLM^{+dIFS}$ increased the EC_{50} of 5-FU by ~5- and ~8-fold compared to in $RPMI^{+IFS}$ and $RPMI^{+dIFS}$, respectively (Figure 7C), without affecting the potency of doxorubicin – a DNA-damaging drug also commonly used in the treatment of cancer (Figure 7D). Moreover, removal of just uric acid from $HPLM^{+dIFS}$ reduced the EC_{50} of 5-FU in NOMO1 cells by nearly 6-fold (Figure 7E), again without affecting doxorubicin sensitivity (Figure 7F). In cells treated with 5-FU and cultured in $HPLM^{+dIFS}$ lacking uric acid, we readily detected FUMP, fluorodeoxyuridine monophosphate (FdUMP), as well as 5-FU (Figure 7G). While culture in uric acid-containing $HPLM^{+dIFS}$ had little effect on the intracellular abundances of FdUMP and 5-FU, it reduced FUMP levels below the limit of detection, consistent with the predicted antagonism of OPRT-mediated FUMP synthesis by orotate (Figure 7G).

As 5-FU is no longer used in the treatment of hematological cancers, we also asked if uric acid affects the 5-FU sensitivity of a more clinically relevant cancer cell line (Longley et al., 2003). As in the six hematological cancer cell lines, culture of the SW620 colorectal cancer cell line in $HPLM^{+dIFS}$ increased the intracellular abundance of orotate (Figure S7A),

indicating that uric acid might also affect the 5-FU sensitivity of these cells. Indeed, removal of just uric acid from HPLM^{+dIFS} reduced the 5-FU EC_{50} of SW620 cells by 3-fold relative to that in HPLM^{+dIFS} (Figure S7B), but did not influence doxorubicin sensitivity (Figure S7C).

Thus, at concentrations found in human plasma, the endogenous metabolite uric acid affects the sensitivity of cancer cells to a common chemotherapeutic (Figure 7H). It is interesting to consider whether manipulations of plasma uric acid levels, such as by administration of uricase (Jeha et al., 2004), could improve the 5-FU sensitivity of human tumors that generate FUMP via OPRT-mediated synthesis.

CONCLUSIONS

Although the impact of environmental factors on cell metabolism is increasingly appreciated, traditional culture media and mouse plasma poorly reflect the metabolite composition of human plasma. Cell culture in a new medium, which better reflects the polar metabolite composition of human plasma (HPLM^{+dIFS}), had widespread effects on cellular metabolism compared to that in established media. Among the most dramatic were alterations in the intracellular abundance of metabolites involved in pyrimidine metabolism. We ultimately traced this effect to uric acid, whose plasma concentration is up to an order of magnitude greater in humans than in most other mammals, including mouse and cow (Álvarez-Lario and Macarrón-Vicente, 2010; Kratzer et al., 2014; Wu et al., 1992). We find that uric acid, at concentrations present in human plasma, is an endogenous inhibitor of UMPS, which catalyzes the final two steps of the de novo pyrimidine biosynthesis pathway. Similar to other small molecule inhibitors of UMPS, uric acid induces an accumulation of orotate, which in turn, antagonizes the metabolism of 5-FU to the fluoronucleotide derivatives that mediate its cytotoxic effects.

Through the use of HPLM, we uncovered a role for an endogenous metabolite that would have been difficult to discover by studying cells cultured in established media or in mouse models (Wu et al., 1994). Although the causes of the many other changes to the metabolic landscape induced by HPLM are unexplained, they do reveal the impact of media composition on cellular metabolism, and suggest the potential to generate HPLM derivatives that reflect plasma metabolite conditions associated with particular pathophysiological states or lifestyles. Moreover, in the future it will be interesting to generate HPLM derivatives with additional components, such as proteins and lipids, at concentrations resembling those of adult human plasma, and to consider how HPLM affects other biological processes, including cellular differentiation. We conclude that HPLM should be of broad utility to study cellular metabolism and may help reveal new tumor-specific liabilities or metabolite-drug interactions that are influenced by environmental metabolic composition.

CONTACT FOR REAGENT AND RESOURCE SHARING

Further information and requests for resources and reagents should be directed to and will be fulfilled by the Lead Contact David M. Sabatini (sabatini@wi.mit.edu).

EXPERIMENTAL MODEL AND SUBJECT DETAILS

Collection of Mouse Plasma

The MIT Institutional Animal Care and Use Committee approved procedures used for the collection of whole blood. Male C57Bl/6J mice, 3.5 months old, were maintained on regular chow at the specific pathogen free animal facility of the Whitehead Institute, and were fasted for 18 hr prior to blood collection. At 10:00 AM, 100 μL of blood was collected into heparinized tubes (Sarstedt Microvette 200 LH) from the facial vein, and the plasma fraction was collected following centrifugation at 850 *g* for 6 min at 4°C.

Collection of Human Plasma

At 6:00 AM, 10 mL of blood from the corresponding author (male, 48 years old) was collected into a heparinized tube (BD Vacutainer 366480) from the antecubital vein. Upon transferring 100 μL of blood to a fresh heparinized tube (Sarstedt Microvette 200 LH), the plasma fraction was collected following centrifugation at 850 *g* for 6 min at 4°C.

Primary cell isolation

A primary human acute myeloid leukemia specimen (estimated blast percentage of 80%; CD33+ CD13+ MPO−, CD117+, CD34+, HLA-DR+, CD71dim+) was collected from the bone marrow of a patient (male, 73 years old) at the Massachusetts General Hospital (MGH) as approved by the MGH Institutional Review Board. To remove red blood cells (RBCs), the specimen was added to a 20X volume of RBC lysis buffer (BioLegend 420301) and mixed well at room temperature. After 15 min incubation, cells were centrifuged at 650 *g* for 5 min at room temperature, resuspended in 5 mL PBS, again centrifuged using the same settings, and finally, resuspended in 2.5 mL PBS.

Cell lines

The following cell lines were kindly provided by: K562 and NOMO1, Dr. James Griffin (Dana Farber Cancer Institute); P12-Ichikawa, Dr. A. Thomas Look (Dana Farber Cancer Institute); SUDHL4, Dr. Margaret Shipp (Dana Farber Cancer Institute); KMS-12-BM and SEM, the Cancer Cell Line Encyclopedia (Broad Institute); CLF-PED-015T, Dr. Andrew Hong (Broad Institute); and BJ, Dr. Nir Hacohen (Broad Institute). Remaining cell lines (786-0, A549, MCF7, and SW620) were purchased from ATCC. Cell lines were verified to be free of mycoplasma contamination (Freshney, 2010) and the identities of all cell lines other than CLF-PED-015T (received at passage 7) and BJ (received at passage 1) were authenticated by STR profiling. We note the STR profile for SW620 cells revealed very minor background at 2 of the 10 loci evaluated, perhaps as a consequence of genetic drift over the course of passaging.

Cell culture conditions

Cells were primarily cultured in the following media:

1. $RPMI^{+IFS}$: RPMI 1640 lacking glucose (Thermo Fisher Scientific 11879020) to which we added 5 mM glucose, 10% heat inactivated fetal bovine serum (IFS), penicillin, and streptomycin.

2. RPMI^{+dIFS}: RPMI 1640 lacking glucose (Thermo Fisher Scientific 11879020) to which we added 5 mM glucose, 10% dialyzed IFS, penicillin, and streptomycin.
3. HPLM^{+dIFS}: HPLM (See Table S1) to which we added 10% dialyzed IFS, RPMI 1640 100X Vitamins (Sigma-Aldrich R7256), penicillin, and streptomycin.

Using SnakeSkin dialysis tubing, 3.5K MWCO, 35 mm (Thermo Fisher Scientific PI88244), IFS was dialyzed against a 20X volume of PBS. Dialysis was carried out for 48 hr at 4°C with a complete PBS exchange every 9–12 hr. Prior to use, all media were sterile filtered using bottle-top vacuum filters, cellulose acetate membrane, pore size 0.45 μm (Sigma-Aldrich CLS430514).

Prior to experiments, cells were grown in the medium of interest for at least two passages unless otherwise noted. Cells were typically split in the range 1:3 to 1:5 into fresh medium. All cells were maintained at 37°C and 5% CO_2.

For the short-term culture of primary AML cells, media were supplemented with 50 μM β-mercaptoethanol (Thermo Fisher Scientific 21985023), 100 ng/mL human SCF (Peprotech 300–07), 10 ng/mL human IL-3 (Peprotech 200–03), 20 ng/mL human IL-6 (Peprotech 200–06), 10ng/mL human TPO (Peprotech 300–18), and 10 ng/mL FLT3L (Peprotech 300–19).

For HEK-293T transfection experiments, cells were cultured in DMEM supplemented with 10% IFS, penicillin, and streptomycin.

METHOD DETAILS

Plasmid construction

All plasmids and primers used in this study are described in Table S4. All plasmids generated in this study are deposited in Addgene.

Construction of lentiviral plasmid pLJC2-Rap2A-3xFLAG—The KRASV12 gene was amplified from the pDONR223-KRASV12 template using the primers JC4/JC5, digested with *AgeI-BamHI*, and cloned into pLJM1-eGFP to generate pLJM1-KRASV12-3xFLAG. Plasmid pLJC1-KRASV12-3xFLAG was constructed using QuickChange PCR to remove two *NotI* sites of pLJM1-KRASV12-3xFLAG with the primers JC48/JC49 and JC50/JC51, respectively. The Rap2A gene was amplified from the pLJM1-Rap2A template using the primers JC68/JC69, digested with *PacI-NotI*, and cloned into pLJC1-KRASV12-3xFLAG to generate pLJC1-Rap2A-3xFLAG. The sequence encoding Rap2A-3xFLAG was then amplified from pLJC1-Rap2A-3xFLAG using the primers JC_LJC2-F/JC79, digested with *AgeI-EcoRI*, and cloned into pLJM1-eGFP to generate pLJM1-Rap2A-3xFLAG. Plasmid pLJC2-Rap2A-3xFLAG was then constructed using QuickChange PCR to remove two *NotI* sites of pLJM1-Rap2A-3xFLAG with the primers JC48/JC49 and JC50/JC51, respectively.

Construction of UMPS plasmids—The UMPS gene was amplified from the pDONR223-UMPS template using the primers JC624/JC625, digested with *PacI-NotI*, and cloned into pLJC2-Rap2A-3xFLAG to generate pLJC2-UMPS-3xFLAG. Plasmid pLJC2-

UMPS (Y37A, R155A)-3xFLAG was constructed using a 2-step protocol based on overlap extension PCR methodology. In the first step, three fragments were amplified from the pLJC2-UMPS-3xFLAG template using the following primer pairs: JC_LJC2-F/JC716, JC715/JC720, and JC719/JC_LJC2-R. In the second step, the three fragments were pooled in a second PCR containing the primers JC_LJC2-F/JC_LJC2-R, then digested with *PacI-NotI*, and cloned into pLJC2-UMPS-3xFLAG.

Design of HPLM

The Human Metabolome Database, which is integrated with the Serum Metabolome Database, (Psychogios et al., 2011; Wishart et al., 2013) contains 2,192 metabolites that were designated as being both detected and quantified in at least one human biofluid. From this collection, we removed molecules that met one of the following manually applied filtering criteria: (1) Metabolites for which a concentration in normal adult human blood was not indicated; (2) Lipophilic metabolites, including fatty acids, cholesterol, and derivatives of the following: cholesterol ester, ceramide, diglyceride, ganglioside, glycerophosphocholine, monoacylglyceride, phosphatidic acid, phosphatidylglycerol, phosphatidylinositol, phosphatidylserine, sphingomyelin, and triglyceride; (3) Metabolites with concentrations in normal adult human blood < 6 μM as denoted by at least one reference source; (4) Metabolites with concentrations in normal adult human blood indicated by only one reference source; and (5) Metabolites that were not commercially available. Although vitamins are among the nutritional requirements of cells in culture (Eagle, 1955c), most had annotated plasma concentrations that were well below the 6 μM threshold we set. Therefore, rather than omit these metabolites, we chose to supplement HPLM with a commercial concentrated mixture of vitamins at concentrations equivalent to those of RPMI 1640. In addition, while trace elements such as copper and zinc are also essential for cells in culture, they are often contributed in sufficient quantities by transport molecules in IFS, such as albumin and insulin, and exceeding their necessary levels is often detrimental to cell proliferation (Sigma-Aldrich Media Expert; Online Resource). Thus, we did not include trace elements among the defined components of HPLM. Additional modifications, such as removal of non-endogenous compounds and gases, were also made to generate the final list of 20 proteinogenic amino acids, 27 additional polar metabolites, and 10 small ions included in the formulation of HPLM at concentrations similar to the calculated average of values reported for normal adult human blood. As anticipated, the metabolite concentrations of plasma collected from the corresponding author (See Collection of Human Plasma; Polar metabolite profiling and quantification of metabolite abundance) largely reflected those of HPLM. See Table S1.

Growth curves

For suspension cells, all cell lines were seeded at a density of 100,000 cells/mL in 12 mL culture medium and grown in 25 cm^2 rectangular canted neck cell culture flasks (Westnet 430639). Cell density measurements were recorded every 9–12 hr using a Beckman Z2 Coulter Counter with a diameter setting of 8–30 μm. For each adherent cell line, 100,000 total cells were seeded in 3 mL culture medium in each of nine technical replicates, and grown in 6-well plates. Every 9–12 hr, one replicate was aspirated, washed in 1 mL PBS, trypsinized, and used to analogously obtain cell density measurements.

Points for time versus natural log-transformed cell density were plotted in GraphPad Prism and those comprising the exponential growth phase were fit using a linear regression equation. Specific growth rates were equivalent to slopes of the fit lines.

Polar metabolite profiling and quantification of metabolite abundance

LC/MS-based analyses were performed on a QExactive benchtop orbitrap mass spectrometer equipped with an Ion Max source and HESI II probe, which was coupled to a Dionex UltiMate 3000 UPLC system (Thermo Fisher Scientific). External mass calibration was performed using the standard calibration mixture every 7 days. Acetonitrile was LC/MS HyperGrade (EMD Millipore). All other solvents were LC/MS Optima grade (Thermo Fisher Scientific).

Media and Plasma—For metabolite profiling of media and plasma, samples were diluted 1:40 in a solution containing 50% methanol, 30% acetonitrile, 20% water and either phenylalanine-d_8 (Cambridge Isotope Laboratories DLM-1372) at 10 ng/mL or a mixture of 17 isotope-labeled amino acids (Cambridge Isotope Laboratories MSK-A2-1.2) each at 909 nM as internal standard(s) (Metabolite Composition of Cultured Media samples) and then stored at −80°C. Following a 5 min vortex and centrifugation at 21130 *g* for 5 min at 4°C, 2 μL of each sample was injected onto a ZIC-pHILIC 2.1 × 150 mm analytical column equipped with a 2.1 × 20 mm guard column (both 5 μm particle size, EMD Millipore). Buffer A was 20 mM ammonium carbonate, 0.1% ammonium hydroxide; buffer B was acetonitrile. The chromatographic gradient was run at a flow rate of 0.150 mL/min as follows: 0–20 min: linear gradient from 80% to 20% B; 20–20.5 min: linear gradient from 20% to 80% B; 20.5–28min: hold at 80% B. The mass spectrometer was operated in full scan, polarity-switching mode with the spray voltage set to 3.0 kV, the heated capillary held at 275°C, and the HESI probe held at 350°C. The sheath gas flow rate was set to 40 units, the auxiliary gas flow was set to 15 units, and the sweep gas flow was set to 1 unit. The MS data acquisition was performed in a range of 70–1000 m/z, with the resolution set to 70,000, the AGC target at 10^6, and the maximum integration time at 20 msec.

Suspension cell lines—For metabolite profiling whole-cell suspension samples, cells were pelleted and then seeded at a density of 200,000 cells/mL in 6-well plates in 3 mL of fresh culture medium. After 24 hr incubation, cells were centrifuged at 250 *g* for 5 min, resuspended in 1 mL ice-cold 0.9% sterile NaCl (Bioexpress MSDW-1000), and again centrifuged at 250 *g* for 5 min at 4°C. Metabolites were extracted in a 1 mL solution of 80% methanol containing 10 ng/mL phenylalanine-d_8 as an internal standard. Following a 10 min vortex and centrifugation for 3 min at 21130 *g* for 10 min at 4°C, samples were dried under nitrogen gas. Dried samples were stored at −80°C and then resuspended in 100 μL water. Following a 10 min vortex and centrifugation at 21130 *g* for 10 min at 4°C, 4 μL of each cell sample was injected for LC/MS analysis as described above for profiling media samples. For all experiments, an additional culture replicate was set up identically and used for measuring cell number and volume, which were each measured using a Beckman Z2 Coulter Counter with a diameter setting of 8–30 μm.

Adherent cell lines—For metabolite profiling whole-cell adherent samples, cells were pelleted and then seeded at one of the following densities in 6-well plates in 3 mL of fresh culture medium: 70,000 cells/mL (786-0); 100,000 cells/mL (A549); 70,000 cells/mL (MCF7); 200,000 cells/mL (SW620); 80,000 cells/mL (BJ); and 100,000 cells/mL (CLF-PED-015T). After 24 hr incubation, wells were aspirated on ice, briefly washed in 1 mL ice-cold 0.9% sterile NaCl, and then extracted in a 1 mL solution of 80% methanol containing 10 ng/mL phenylalanine-d_8 as an internal standard. Subsequent steps were identical to those described above for profiling suspension cell samples. For CLF-PED-015T, cells were grown in the medium of interest for two passages prior to profiling to minimize the passage number at which they were profiled.

Primary AML cells—Following RBC removal from the primary leukemia specimen (See Primary Cell Isolation), a 1 mL aliquot of isolated cells was centrifuged at 21130 *g* for 15 sec, resuspended in 10 mL of culture medium ($RPMI^{+IFS}$ or $HPLM^{+dIFS}$) supplemented with human cytokines (See Cell Culture Conditions), and seeded equivalently across four wells of a 6-well plate. After 8 hr incubation, cells were pooled, centrifuged at 21130 *g* for 15 sec, and resuspended in 1 mL ice-cold 0.9% NaCl. From this resuspension, 100 μL was used to obtain the number and volume of viable cells in each sample using a Beckman Z2 Coulter Counter with a diameter setting of 5–24 μm. The remainder of cells were centrifuged at 21130 *g* for 15 sec, and then extracted in a 1 mL solution of 80% methanol containing 10 ng/mL phenylalanine-d_8 as an internal standard. Subsequent steps were identical to those described above for profiling suspension cell samples.

NAD/NADH—For metabolite profiling whole-cell suspension samples to specifically quantify NAD and NADH, cells were pelleted and then seeded at a density of 200,000 cells/mL in 6-well plates in 3 mL of fresh culture medium. After 24 hr incubation, cells were centrifuged at 250 *g* for 5 min, resuspended in 1 mL ice-cold 0.9% sterile NaCl, and again centrifuged at 250 *g* for 5 min at 4°C. Metabolites were extracted in a 500 μL solution of 80% methanol containing 10 ng/mL phenylalanine-d_8 as an internal standard. Following a 10 min vortex and centrifugation for 3 min at 21130 *g* for 10 min at 4°C, samples were immediately injected for LC/MS analysis as described for whole-cell samples otherwise.

Metabolite profiling of UMPS Activity Assay—For metabolite profiling of UMPS activity assay samples, reaction mixtures were extracted (See UMPS Activity Assay) and 5 μL of each sample was injected for LC/MS analysis as described otherwise, except that the mass spectrometer was operated in full scan, negative ionization mode only.

5-FU Treatment—NOMO1 cells were pelleted and then seeded at a density of 200,000 cells/mL in 6-well plates in 3 mL of culture medium containing 20 μM 5-FU. After 24 hr incubation, metabolite extractions were performed identically to those described above for profiling suspension cell samples.

Quantification—A list of nearly 170 metabolites encompassing a variety of metabolic pathways and processes was created with the intention of exploring the metabolome in a global and targeted fashion. From a library of chemical standards assembled by the Whitehead Institute Metabolite Profiling core facility, we constructed six pools of standards

(See Table S1 for the composition of each pool) that together accounted for nearly 90% of this list. Standards were validated by LC/MS to confirm that they generated robust peaks at the expected *m/z* ratio. Stock solutions of each pool, containing 1 mM of each metabolite in water, were stored at −80°C. On the day of each run, these stocks were serially diluted in water, further diluted 1:10 into appropriate extraction solution, and then run in parallel with a given batch of biological samples.

Metabolite identification and quantification were performed with XCalibur QuanBrowser 2.2 (Thermo Fisher Scientific) using a 10 ppm mass accuracy window and 0.5 min retention time window. To confirm metabolite identities and to enable quantification, the aforementioned pools of metabolite chemical standards were used. Typically, the final concentrations of standards were 10 nM, 100 nM, 1 μM, 10 μM, and 100 μM. For glucose, chemical standard solutions were also made at concentrations of 125 μM and 250 μM. For NAD and NADH, standards at 10 nM were omitted. For certain metabolites, chemical standards were utilized only for metabolite identification. For those metabolites lacking a chemical standard, peak identification was restricted to high confidence peak assignments (Smith et al., 2005). See Table S1.

Because metabolite extraction protocols differed by sample type, the concentration of phenylalanine-d_8 in processed samples varied: chemical standard pools (9 ng/mL), media and plasma samples (9.75 ng/mL), and cell samples (100 ng/mL). Therefore, the raw peak area of phenylalanine-d_8 within each sample of a given batch was first normalized to account for these differences. To quantitate metabolites, we first divided the raw peak area of each metabolite by its corresponding normalized phenylalanine-d_8 peak area. From the normalized metabolite peak areas of a given chemical standard, we then generated a corresponding standard curve fit to a quadratic log-log equation, typically with $r^2 > 0.95$, which was used to determine the metabolite concentration in each biological metabolite extract. The total number of moles of a metabolite in a particular whole-cell or medium/plasma extract was then calculated from the sample concentration and the corresponding sample volume. Thus, final metabolite concentrations in biological samples were calculated using the appropriate equation below:

$$\begin{gathered}\text{Media and plasma samples: Concentration by standard} \times 40 \\ \text{Whole- cell samples: Concentration by standard curve} \times 100/(\text{cell volume, in } \mu\text{L}) \\ \text{Whole- cell NAD/NADH samples: Concentration by standard curve} \times 500/(\text{cell volume, in } \mu\text{L})\end{gathered}$$

For those metabolites that were not quantified using a standard curve, normalized peak areas were used in the above calculations. For whole-cell profiles of adherent cell lines and primary AML cells, normalized peak areas were used for all metabolites.

Highly targeted metabolomics—For the highly targeted analyses of FdUMP and FUMP in whole-cell samples following 5-FU treatment, the instrument was run as described (See Media and Plasma), but with an additional tSIM (targeted selected ion monitoring) scan in negative ionization mode. The tSIM settings were as follows: resolution set to 70,000, an AGC target of 10^5, and a maximum integration time of 250 msec. The target masses were

325.0243 (corresponding to FdUMP) and 341.0192 (corresponding to FUMP). The isolation window around each target mass was set to 1.0 m/z.

For orotate, PRPP, OMP, and UMP in UMPS assay samples, all settings as described for the tSIM scan used for FdUMP and FUMP were identical except that the maximum integration time was 200 msec, and the target masses were 155.0098 (corresponding to orotate), 323.0286 (corresponding to UMP), 367.0184 (corresponding to OMP), and 388.9445 (corresponding to PRPP).

For NAD and NADH in whole-cell samples, all settings as described for the tSIM scan used for FdUMP and FUMP were identical except that the target masses were 662.1019 (corresponding to NAD) and 664.1175 (corresponding to NADH).

For carbamoylaspartate, orotate, and orotidine in primary AML whole-cell samples, all settings as described for the tSIM scan used for FdUMP and FUMP were identical except that the target masses were 175.036 (corresponding to carbamoylaspartate), 155.0098 (corresponding to orotate), and 287.0521 (corresponding to orotidine).

For pyruvate and succinate in media samples profiled following 24 hr cell culture, all settings as described for the tSIM scan used for FdUMP and FUMP were identical except that the target masses were 87.0088 (corresponding to pyruvate) and 117.0193 (corresponding to succinate).

Labeling experiments

Cells were pelleted and then seeded at a density of 200,000 cells/mL in 6-well plates in 3 mL of culture medium containing either 5 mM [U-^{13}C]-glucose or 550 μM [α-^{15}N]-glutamine. After 24 hr incubation, metabolite extractions were performed identically to those described for profiling suspension cell samples (See Polar metabolite profiling and quantification of metabolite abundance).

For [α-^{15}N]-glutamine tracing studies, the RPMI media were prepared using SILAC RPMI 1640 Flex Media (Thermo Fisher Scientific A2494201), to which we added 5 mM glucose, 14 μM phenol red, 1.15 mM arginine, 270 μM lysine, penicillin, streptomycin, and [α-^{15}N]-glutamine at the concentration noted above.

Lipidomics of culture media

LC/MS-based analyses were performed using the same QExactive benchtop orbitrap mass spectrometer and Dionex UltiMate 3000 UPLC system described otherwise (See Polar metabolite profiling and quantification of metabolite abundance).

For lipid profiling of media, 95 μL methanol and 190 μL dichloromethane were sequentially mixed by 20 sec vortex with 15 μL of medium. Following addition of 60 μL water to the mixture, samples were vortexed for 10 min at 4°C, and then centrifuged at 8000 *g* for 10 min at 4°C. From the resulting two-phase solution, 100 μL of the bottom (lipid) fraction was carefully collected and dried under nitrogen gas. Dried samples were stored at −80°C and then resuspended in a 50 μL solution of 65% acetonitrile, 30% isopropanol, and 5% water.

Following a 10 min vortex and centrifugation at 21130 *g* for 5 min at 4°C, 5 μL was injected onto an Ascentis Express C18 2.1 × 150 mm 2.7 μm column (Sigma-Aldrich).

Buffer A was a solution of 60% water, 40% acetonitrile, 10 mM ammonium formate (Sigma-Aldrich), and 0.1% formic acid (Pierce); buffer B was a solution of 90% isopropanol, 10% acetonitrile, 10 mM ammonium formate, and 0.1% formic acid. The chromatographic gradient was run at a flow rate of 0.260 mL/min as described previously ((Hu et al., 2008): 0–1.5 min, isocratic elution with 32% B; from 1.5 to 4 min, increase to 45% B; from 4 to 5 min, to 52% B; from 5 to 8 min, to 58% B; from 8 to 11 min, to 66% B; from 11 to 14 min, to 70% B; from 14 to 18 min, to 75% B; from 18 to 21 min, to 97% B; from 21 to 25 min, maintain at 97% B; from 25 to 25.1 min, decrease to 32% B and maintain for an additional 4.9 min for column re-equilibration. The column oven and autosampler tray were held at 55°C and 4°C, respectively. Separate injections for positive and negative ionization modes were made for each sample. The spray voltage was set to 4.2 kV and the heated capillary and HESI were held at 320°C and 300°C, respectively. The S-lens RF level was set to 50, and the sheath and auxiliary gas were set to 35 and 3 units, respectively. These conditions were held constant for both positive and negative ionization mode acquisitions. The MS data acquisition was performed in a full scan/data-dependent MS^2 mode. For the full scan acquisition, the resolution was set to 70,000, the AGC target at 10^6, the maximum integration time at 50 msec, and the scan range was 133.4–2000 m/z.

High-throughput identification and relative quantification of lipids was performed separately for positive and negative ionization mode data using LipidSearch software (Thermo Fisher Scientific) (Taguchi and Ishikawa, 2010; Yamada et al., 2013) using the default parameters for QExactive Product Search and Alignment. After alignment, raw peak areas for all identified lipids were exported to Microsoft Excel and filtered according to the following pre-determined quality control criteria: Rej (“Reject” parameter calculated by LipidSearch software) equal to 0; PQ (“Peak Quality” parameter calculated by LipidSearch software) greater than 0.85; CV (standard deviation divided by the average peak area across triplicate injections of a representative pooled biological sample) below 0.4; R (linear correlation across a three-point dilution series of the representative pooled sample) greater than 0.9. Raw peak areas of the filtered lipids were added to generate a “total lipid signal” for each sample, and individual lipid peak areas were normalized to this total signal as a control for extraction efficiency and sample loading. Normalized peak areas for all filtered lipids designated within a particular lipid class were then summed to represent the total signal of that class in the sample. Finally, for free fatty acids, peak areas were obtained using XCalibur QuanBrowser 2.2 (See Polar metabolite profiling and quantification of metabolite abundance) and normalized using the “total lipid signal” for the corresponding sample as well. See Table S1.

Cholesterol Quantification

Concentrations of total, LDL, and HDL cholesterol in IFS and dIFS were measured via enzymatic methods by the Yale Mouse Metabolic Phenotyping Center Analytical Core using a Cobas Mira Plus Analyzer (Roche Diagnostics). For total cholesterol, 3 μL of sample was added to 275 μL Cholesterol Rapid Liquid Reagent (Cliniqa R85464) and incubated at 37°C

for 10 min prior to measurement of the absorbance at 500nm. For HDL cholesterol, 3 μL of sample was added to 180 μL HDL Cholesterol Direct Reagent 1 (Cliniqa R85549) and 60 μL HDL Cholesterol Direct Reagent 2 (Cliniqa R85549) and incubated at 37°C for 10 min prior to measurement of the absorbance at 600nm. For LDL cholesterol, 3 μL of sample was added to 225 μL LDL Direct Reagent 1 (Cliniqa R85556) and 75 μL LDL Direct Reagent 2 (Cliniqa R85556) and incubated at 37°C for 10 min prior to measurement of the absorbance at 600nm. For quantification purposes, the Cobas analyzer was calibrated using two chemical controls.

Net exchange rates

At each time point that cell density was measured during the construction of a particular growth curve, a small aliquot of the culture was carefully removed, centrifuged at 250 *g* for 5 min at 4°C, and metabolites were extracted from the supernatant as described for media and plasma samples, and then stored at −80°C (See Polar Metabolite Profiling and Metabolite Quantification). For a given growth curve, we profiled an extraction sample associated with a time point that fell in mid-exponential phase. We also profiled fresh media in parallel and the specific exchange rate for a given metabolite was obtained according to the simplified Monod model, $q = \mu/Y_{X/S}$, which expands to: $q = \mu \times V \times (\Delta M/\Delta X)$, where μ is the specific growth rate, V is the culture volume, ΔM is the difference in metabolite concentration between the two time points, and ΔX is the difference in cell density between the two time points.

Metabolite composition of cultured media

Cells were pelleted and then seeded at a density of 200,000 cells/mL in 6-well plates in 3 mL of fresh culture medium. After 24 hr incubation, a 100 μL aliquot of the culture was collected and centrifuged at 250 *g* for 5 min. Metabolites were then extracted from the supernatant as described for media and plasma samples, and then stored at −80°C (See Polar Metabolite Profiling and Metabolite Quantification).

Expression and Immunopurification of recombinant UMPS

For transfection of HEK-293T cells, 4 million cells were plated in 15 cm culture dishes. After 24 hr, cells were transfected with 15 μg of pLJC2-UMPS-3xFLAG or pLJC2-UMPS (Y37A, R155A)-3xFLAG using the polyethylenimine method (Boussif et al., 1995). After 48 hr, cells were rinsed once with ice-cold PBS and then immediately lysed with lysis buffer (1% Triton X-100, 40 mM Tris-HCl pH 7.5, 100 mM NaCl, 5 mM $MgCl_2$, 1 tablet of EDTA-free protease inhibitor (Roche 11580800; per 25 mL buffer), 1 tablet of PhosStop phosphatase inhibitor (Roche 04906845001; per 10 mL buffer)). The cell lysates were cleared by centrifugation at 21130 *g* for 10 min at 4°C. For anti-FLAG immunoprecipitation, the FLAG-M2 affinity gel (Sigma A2220) was washed 3 times in lysis buffer. For each experiment, 500 μL of a 50/50 slurry of the affinity gel was then added to a pool of clarified lysates collected from 5 individual 15 cm culture dishes, and incubated with rotation for 3 hr at 4°C. Following immunoprecipitation, the beads were washed 2 times in lysis buffer and 3 times with lysis buffer containing 500 mM NaCl. Recombinant protein was then eluted in lysis buffer containing 1 mg/mL FLAG peptide for 1 hr at 4°C. The eluent was isolated by centrifugation at 100 *g* for 4 min at 4°C (BioRad micro bio-spin column 732-6204), buffer

exchanged (Amicon Ultra 30K NMWL) against 20 volumes of storage buffer (40 mM Tris-HCl pH 7.5, 100 mM NaCl, 1.5 mM dTT), mixed with glycerol (final concentration 15% v/v), and finally snap-frozen with liquid nitrogen and stored at −80°C. Protein samples were quantified using Bradford reagent (Bio-Rad) and a BSA standard, and verified by 12% SDS-PAGE.

UMPS Activity Assay

Reactions of each purified UMPS variant (20–40 nM enzyme) with orotate (100 μM) and PRPP (300 μM) were carried out at 37° C in 20 mM Tris-HCl pH 7.5, 5 mM Na_2HPO_4, 5 mM $MgCl_2$, 2 mM dTT, 100 μM EDTA (adapted from (Han et al., 1995)), and various concentrations of putative inhibitors in a total volume of 100 μL. Following 20 min incubation, a 15 μL aliquot of the reaction mixture was removed and immediately added to 85 μL ice-cold 80% methanol for metabolite extraction, vortexed for 5 min, and centrifuged at 21130 *g* for 1 min at 4°C.

Stock solutions of 6-azauridine (Sigma-Aldrich A1882), 6-aza-UMP (Santa Cruz sc-291171), 9-methyluric acid (Santa Cruz sc-362184), allantoin (Sigma-Aldrich 05670), allopurinol (Sigma-Aldrich PHR1377), and uric acid (Sigma-Aldrich U2625) were made up fresh at 200 mM in 1 M NaOH, and upon appropriate dilutions, had little effect on reaction pH.

Using the peak areas of a UMP chemical standard (final concentrations 625 nM, 1.25 μM, 2.5 μM, 5 μM, and 10 μM) identically prepared in 80% methanol, we generated a standard curve fit to a linear equation to ensure that UMP concentrations in the reaction samples did not exceed 10% of the initial orotate concentration. An OMP chemical standard was not available.

Drug Treatments

NOMO1 cells were seeded at a density of 16,667 cells/mL in 6-well plates in 3 mL of culture medium. After 24 hr incubation, cells were treated with 5-FU (Sigma-Aldrich F6627) (100 nM, 1 μM, 10 μM, 100 μM, or 1 mM) or doxorubicin (Sigma-Aldrich 44583) (1.95 nM, 7.81 nM, 31.25 nM, 125 nM, or 500 nM). All wells, including untreated controls, contained 0.5% DMSO. Following addition of drugs, plates were gently shaken for 2 min. After 4 days of treatment, 200 μL from each well was transferred to a white 96-well plate (Greiner) and cell viability was assessed with Cell Titer-Glo (Promega). Luminescence was measured with a SpectraMax M5 Plate Reader (Molecular Devices) and normalized to an untreated control.

SW620 cells were seeded in white 96-well plates (Greiner) at a density of 2000 cells/well and allowed to attach for 24 hr. 5-FU and doxorubicin were prepared in DMSO and dispensed using an HP D300 compound dispenser. Cell viability was assessed with Cell-Titer Glo at 4 days following treatment and luminescence was measured as described above.

Dose-response values were plotted in GraphPad Prism and fit using a One Site-Fit logIC50 equation.

Cell lysis and immunoblotting

To evaluate mTORC1 signaling, cells cultured in a given medium were pelleted and then seeded in each of three wells of a 6-well plate at a density of 333,000/mL in 3 mL of corresponding fresh culture medium. After 2 hr incubation, cells were pooled, centrifuged at 250 *g* for 5 min, resuspended in 1 mL ice-cold PBS, and again centrifuged at 250 *g* for 5 min at 4°C. Cells were then immediately lysed with lysis buffer (1% Triton X-100, 10 mM β-glycerol phosphate, 10 mM pyrophosphate, 40 mM HEPES pH 7.4, 2.5 mM $MgCl_2$, and 1 table of EDTA-free protease inhibitor). The cell lysates were cleared by centrifugation at 21130 *g* for 10 min at 4°C and then quantified for protein concentration using Bradford reagent. Protein samples were normalized for protein content, denatured by the addition of Laemmli buffer, boiled for 5 min, resolved by 8% SDS-PAGE, and transferred to a polyvinyl difluoride membrane (Millipore).

Membranes were blocked with 5% nonfat dry milk prepared in TBST for 1 hr at room temperature, then incubated with primary antibodies in 5% BSA overnight at 4°C. Primary antibodies to the following proteins were used at the indicated dilutions: Raptor (EMD Millipore 09-217; 1:1000); S6 kinase (Cell Signaling Technology 2708; 1:5000); and Phospho-S6 kinase (Thr389) (Cell Signaling Technology 9234; 1:1000). Membranes were washed with TBST three times for 5 min each, and then incubated with secondary antibody (Goat anti-Rabbit IgG HRP, Santa Cruz sc-2054; 1:5000) in 5% nonfat dry milk for 1 hr at room temperature. Membranes were washed again with TBST three times for 5 min each, and then visualized using chemiluminescence (Thermo Fisher Scientific).

Virus production and transduction efficiency

For transfection of HEK-293T cells, pLJM1-eGFP was co-transfected with the VSV-G envelope plasmid and the Delta-VPR lentiviral packaging plasmid using XTremeGene 9 Transfection Reagent (Roche). Culture medium was exchanged 16 hr after transfection with the same medium instead supplemented with 20% IFS. The virus-containing supernatant was collected 48 hr after transfection and passed through a 0.45 μm filter to eliminate cells.

K562 cells were infected with eGFP lentivirus in culture medium containing 8 μg/mL polybrene (EMD Millipore) by centrifugation at 1200 *g* for 45 min at 37°C. After 24 hr incubation, cells were pelleted to remove virus and re-seeded into fresh culture medium. The efficiencies of transduction were evaluated 96 hr after infection by FACS (BD LSR Flow Cytometer) with gates applied to live cells that were GFP-positive.

Seahorse analysis

Oxygen consumption of intact cells was measured using an XF24 Extracellular Flux Analyzer (Seahorse Bioscience). XF24 Cell Culture Microplates (Seahorse Bioscience) were coated with a solution containing 0.08 mg/mL Cell-Tak (Corning), 90 μM $NaHCO_3$, and 33 μM NaOH to increase suspension cell adherence. After 20 min, all wells were washed twice with sterile water, and then seeded with either 200,000 (P12-Ichikawa, NOMO1, SEM) or 125,000 (SUDHL4) total cells in a volume of 500 μL. Cells were attached by centrifugation at 600 *g* for 10 min with no brake, transferred to an incubator lacking CO_2 for 30 min, and then transferred to a standard incubator. After 16 hr, basal oxygen consumption rates were

determined on the XF24 Analyzer and normalized by cell number as measured following the assay using a Beckman Z2 Coulter Counter with a diameter setting of 8–30 μm.

QUANTIFICATION AND STATISTICAL ANALYSIS

All p values were calculated using a two-tailed unpaired *t* test in GraphPad Prism 6. All CV and R values calculated for filtering lipids identified in LipidSearch were determined in Microsoft Excel. All specific growth rates and r values describing the relationship between rates of glucose consumption and lactate secretion were derived from linear regression analyses performed in GraphPad Prism 6. The exact value of n and the definition of center and precision measures are provided in all figure legends. All instances where n replicates are reported had n biological replicates, except the metabolite profiling data described for primary AML, for which n instead denotes technical replicates.

DATA AND SOFTWARE AVAILABILITY

Data resources

Datasets can be found in Tables S1, S2, and S3.

Supplementary Material

Refer to Web version on PubMed Central for supplementary material.

Acknowledgments

We thank W.W. Chen, B.P. Fiske, M.A. Keibler, V. Nardi, M.E. Pacold, and J.P. Ray for helpful suggestions; T. Kunchok for assistance in preparing the chemical standard pools; B. Chan for assistance with LipidSearch; J.D. Griffin, A.L. Hong, N. Hacohen, A.T. Look, and M.A. Shipp for kindly providing cell lines. This work was supported by grants from the US NIH (R01 CA103866 and R37 AI047389) and the Koch Institute (Frontier Research Grant) to D.M.S.; and from the Department of Defense (W81XWH-15-1-0337) to E.F. Fellowship support was provided by the American Cancer Society (PF-12-099-01-TBG) and the Koch Institute (Ludwig Postdoctoral Fellowship) to J.R.C.; by EMBO (Long-Term Fellowship ALTF 1-2014) to M.A.-R.; and by EMBO (Long-Term Fellowship ALTF 350-2012) and the AACR (16-40-38-KANA) to N.K. D.M.S. is an investigator of the Howard Hughes Medical Institute.

References

Adelman R, Saul RL, Ames BN. Oxidative damage to DNA: relation to species metabolic rate and life span. Proc Natl Acad Sci U S A. 1988; 85:2706–2708. [PubMed: 3128794]

Atkinson DE. Energy charge of the adenylate pool as a regulatory parameter. Interaction with feedback modifiers. Biochemistry. 1968; 7:4030–4034. [PubMed: 4972613]

Álvarez-Lario B, Macarrón-Vicente J. Uric acid and evolution. Rheumatology. 2010; 49:2010–2015. [PubMed: 20627967]

Bailey CJ. Orotic aciduria and uridine monophosphate synthase: A reappraisal. J Inherit Metab Dis. 2009; 32:227–233.

Birsoy K, Possemato R, Lorbeer FK, Bayraktar EC, Thiru P, Yucel B, Wang T, Chen WW, Clish CB, Sabatini DM. Metabolic determinants of cancer cell sensitivity to glucose limitation and biguanides. Nature. 2014; 508:108–12. [PubMed: 24670634]

Bobulescu IA, Moe OW. Renal Transport of Uric Acid: Evolving Concepts and Uncertainties. Adv Chronic Kidney Dis. 2012; 19:358–371. [PubMed: 23089270]

Bono VH Jr, Weissman SM, Frei E III . The Effect of 6-Azauridine Administration on De Novo Pyrimidine Production in Chronic Myelogenous Leukemia. J Clin Invest. 1964; 43:1486–1494. [PubMed: 14192530]

Boroughs LK, DeBerardinis RJ. Metabolic pathways promoting cancer cell survival and growth. Nat Cell Biol. 2015; 17:351–359. [PubMed: 25774832]

Boussif O, Lezoualc'h F, Zanta MA, Mergny MD, Scherman D, Demeneix B, Behr JP. A versatile vector for gene and oligonucleotide transfer into cells in culture and in vivo: polyethylenimine. Proc Natl Acad Sci U S A. 1995; 92:7297–7301. [PubMed: 7638184]

Cairns RA, Harris IS, Mak TW. Regulation of cancer cell metabolism. Nat Rev Cancer. 2011; 11:85–95. [PubMed: 21258394]

Cantor JR, Sabatini DM. Cancer cell metabolism: one hallmark, many faces. Cancer Discov. 2012; 2:881–898. [PubMed: 23009760]

Chandrasekera PC, Pippin JJ. Of rodents and men: species-specific glucose regulation and type 2 diabetes research. ALTEX. 2014; 31:157–176. [PubMed: 24270692]

Comerford SA, Huang Z, Du X, Wang Y, Cai L, Witkiewicz AK, Walters H, Tantawy MN, Fu A, Manning HC, et al. Acetate Dependence of Tumors. Cell. 2014; 159:1591–1602. [PubMed: 25525877]

Commisso C, Davidson SM, Soydaner-Azeloglu RG, Parker SJ, Kamphorst JJ, Hackett S, Grabocka E, Nofal M, Drebin JA, Thompson CB, et al. Macropinocytosis of protein is an amino acid supply route in Ras-transformed cells. Nature. 2013; 497:633–637. [PubMed: 23665962]

Davidson SM, Papagiannakopoulos T, Olenchock BA, Heyman JE, Keibler MA, Luengo A, Bauer MR, Jha AK, O'Brien JP, Pierce KA, et al. Environment Impacts the Metabolic Dependencies of Ras-Driven Non-Small Cell Lung Cancer. Cell Metab. 2016; 23:517–528. [PubMed: 26853747]

DeBerardinis RJ, Chandel NS. Fundamentals of cancer metabolism. Sci Adv. 2016; 2:e1600200. [PubMed: 27386546]

DeBerardinis RJ, Lum JJ, Hatzivassiliou G, Thompson CB. The Biology of Cancer: Metabolic Reprogramming Fuels Cell Growth and Proliferation. Cell Metab. 2008; 7:11–20. [PubMed: 18177721]

Demetrius L. Of mice and men. EMBO Rep. 2005; 6:S39–S44. [PubMed: 15995660]

DeNicola GM, Cantley LC. Cancer's Fuel Choice: New Flavors for a Picky Eater. Mol Cell. 2015; 60:514–523. [PubMed: 26590711]

Dulbecco R, Freeman G. Plaque production by the polyoma virus. Virology. 1959; 8:396–397. [PubMed: 13669362]

Eagle H. The specific amino acid requirements of a human carcinoma cell (Stain HeLa) in tissue culture. J Exp Med. 1955a; 102:37–48. [PubMed: 14392239]

Eagle H. The specific amino acid requirements of a mammalian cell (strain L) in tissue culture. J Biol Chem. 1955b; 214:839–852. [PubMed: 14381421]

Eagle H. Nutrition needs of mammalian cells in tissue culture. Science. 1955c; 122:501–514. [PubMed: 13255879]

Eagle H. Amino Acid Metabolism in Mammalian Cell Cultures. Science. 1959; 130:432–437. [PubMed: 13675766]

Eason K, Sadanandam A. Molecular or Metabolic Reprograming: What Triggers Tumor Subtypes? Cancer Res. 2016; 76:5195–5200. [PubMed: 27635042]

Elsea SH, Lucas RE. The mousetrap: what we can learn when the mouse model does not mimic the human disease. ILAR J. 2002; 43:66–79. [PubMed: 11917158]

Evans DR, Guy HI. Mammalian Pyrimidine Biosynthesis: Fresh Insights into an Ancient Pathway. J Biol Chem. 2004; 279:33035–33038. [PubMed: 15096496]

Fallon HJ, Frei E, Block J, Seegmiller JE. The uricosuria and orotic aciduria induced by 6-azauridine. J Clin Invest. 1961; 40:1906–1914. [PubMed: 13891472]

Favaro E, Bensaad K, Chong MG, Tennant DA, Ferguson DJP, Snell C, Steers G, Turley H, Li J-L, Günther UL, et al. Glucose Utilization via Glycogen Phosphorylase Sustains Proliferation and Prevents Premature Senescence in Cancer Cells. Cell Metab. 2012; 16:751–764. [PubMed: 23177934]

Fox RM, Royse-Smith D, O'Sullivan WJ. Orotidinuria induced by allopurinol. Science. 1970; 168:861–862. [PubMed: 5444063]

Fox RM, Wood MH, Royse-Smith D. Hereditary orotic aciduria: types I and II. Am J Med. 1973; 55:791–798. [PubMed: 4753642]

Freshney, RI. A Manual of basic technique and specialized applications. 6. Hoboken, NJ, USA: John Wiley & Sons, Inc; 2010. Culture of Animal Cells.

Han BD, Livingstone LR, Pasek DA, Yablonski MJ, Jones ME. Human uridine monophosphate synthase: baculovirus expression, immunoaffinity column purification and characterization of the acetylated amino terminus. Biochemistry. 1995; 34:10835–10843. [PubMed: 7662663]

Handschumacher RE. Orotidylic acid decarboxylase: inhibition studies with azauridine 5′-phosphate. J Biol Chem. 1960; 235:2917–2919. [PubMed: 13711194]

Hensley CT, Faubert B, Yuan Q, Lev-Cohain N, Jin E, Kim J, Jiang L, Ko B, Skelton R, Loudat L, et al. Metabolic Heterogeneity in Human Lung Tumors. Cell. 2016; 164:681–694. [PubMed: 26853473]

Hong AL, Tseng Y-Y, Cowley GS, Jonas O, Cheah JH, Kynnap BD, Doshi MB, Oh C, Meyer SC, Church AJ, et al. Integrated genetic and pharmacologic interrogation of rare cancers. Nat Commun. 2016; 7:11987. [PubMed: 27329820]

Hosios AM, Hecht VC, Danai LV, Johnson MO, Rathmell JC, Steinhauser ML, Manalis SR, Vander Heiden MG. Amino Acids Rather than Glucose Account for the Majority of Cell Mass in Proliferating Mammalian Cells. Dev Cell. 2016a; 36:540–549. [PubMed: 26954548]

Hu C, van Dommelen J, van der Heijden R, Spijksma G, Reijmers TH, Wang M, Slee E, Lu X, Xu G, van der Greef J, et al. RPLC-Ion-Trap-FTMS Method for Lipid Profiling of Plasma: Method Validation and Application to p53 Mutant Mouse Model. J Proteome Res. 2008; 7:4982–4991. [PubMed: 18841877]

Hu J, Locasale JW, Bielas JH, O'Sullivan J, Sheahan K, Cantley LC, Vander Heiden MG, Vitkup D. Heterogeneity of tumor-induced gene expression changes in the human metabolic network. Nat Biotechnol. 2013; 31:522–529. [PubMed: 23604282]

Jain M, Nilsson R, Sharma S, Madhusudhan N, Kitami T, Souza AL, Kafri R, Kirschner MW, Clish CB, Mootha VK. Metabolite Profiling Identifies a Key Role for Glycine in Rapid Cancer Cell Proliferation. Science. 2012; 336:1040–1044. [PubMed: 22628656]

Jeha S, Kantarjian H, Irwin D, Shen V, Shenoy S, Blaney S, Camitta B, Pui C-H. Efficacy and safety of rasburicase, a recombinant urate oxidase (Elitek™), in the management of malignancy-associated hyperuricemia in pediatric and adult patients: final results of a multicenter compassionate use trial. Leukemia. 2004; 19:34–38.

Jones ME. Pyrimidine nucleotide biosynthesis in animals: genes, enzymes, and regulation of UMP biosynthesis. Annu Rev Biochem. 1980; 49:253–279. [PubMed: 6105839]

Kamphorst JJ, Nofal M, Commisso C, Hackett SR, Lu W, Grabocka E, Vander Heiden MG, Miller G, Drebin JA, Bar-Sagi D, et al. Human Pancreatic Cancer Tumors Are Nutrient Poor and Tumor Cells Actively Scavenge Extracellular Protein. Cancer Res. 2015; 75:544–553. [PubMed: 25644265]

Kand'ár R, Záková P. Allantoin as a marker of oxidative stress in human erythrocytes. Clin Chem Lab Med. 2008; 46:1270–1274. [PubMed: 18636793]

Keibler MA, Wasylenko TM, Kelleher JK, Iliopoulos O, Vander Heiden MG, Stephanopoulos G. Metabolic requirements for cancer cell proliferation. Cancer Metab. 2016; 4:16. [PubMed: 27540483]

Kelley WN, Beardmore TD. Allopurinol: alteration in pyrimidine metabolism in man. Science. 1970; 169:388–390. [PubMed: 5450375]

Kratzer JT, Lanaspa MA, Murphy MN, Cicerchi C, Graves CL, Tipton PA, Ortlund EA, Johnson RJ, Gaucher EA. Evolutionary history and metabolic insights of ancient mammalian uricases. Proc Natl Acad Sci U S A. 2014; 111:3763–3768. [PubMed: 24550457]

Lehuede C, Dupuy F, Rabinovitch R, Jones RG, Siegel PM. Metabolic Plasticity as a Determinant of Tumor Growth and Metastasis. Cancer Res. 2016; 76:5201–5208. [PubMed: 27587539]

Longley DB, Harkin DP, Johnston PG. 5-fluorouracil: mechanisms of action and clinical strategies. Nat Rev Cancer. 2003; 3:330–338. [PubMed: 12724731]

Lunt SY, Vander Heiden MG. Aerobic Glycolysis: Meeting the Metabolic Requirements of Cell Proliferation. Annu Rev Cell Dev Biol. 2011; 27:441–464. [PubMed: 21985671]

MacIver NJ, Michalek RD, Rathmell JC. Metabolic Regulation of T Lymphocytes. Annu Rev Immunol. 2013; 31:259–283. [PubMed: 23298210]

Maddocks ODK, Berkers CR, Mason SM, Zheng L, Blyth K, Gottlieb E, Vousden KH. Serine starvation induces stress and p53-dependent metabolic remodelling in cancer cells. Nature. 2013; 493:542–546. [PubMed: 23242140]

Martignoni M, Groothuis GMM, de Kanter R. Species differences between mouse, rat, dog, monkey and human CYP-mediated drug metabolism, inhibition and induction. Expert Opin Drug Metab Toxicol. 2006; 2:875–894. [PubMed: 17125407]

Mashimo T, Pichumani K, Vemireddy V, Hatanpaa KJ, Singh DK, Sirasanagandla S, Nannepaga S, Piccirillo SG, Kovacs Z, Foong C, et al. Acetate Is a Bioenergetic Substrate for Human Glioblastoma and Brain Metastases. Cell. 2014; 159:1603–1614. [PubMed: 25525878]

Mayers JR, Torrence ME, Danai LV, Papagiannakopoulos T, Davidson SM, Bauer MR, Lau AN, Ji BW, Dixit PD, Hosios AM, et al. Tissue of origin dictates branched-chain amino acid metabolism in mutant Kras-driven cancers. Science. 2016; 353:1161–1165. [PubMed: 27609895]

Moore GE, Gerner RE, Franklin HA. Culture of normal human leukocytes. JAMA. 1967; 199:519–524. [PubMed: 4960081]

Murrell GAC, Rapeport WG. Clinical Pharmacokinetics of Allopurinol. Clin Pharmacokinet. 1986; 11:343–353. [PubMed: 3536254]

Oda M, Satta Y, Takenaka O, Takahata N. Loss of urate oxidase activity in hominoids and its evolutionary implications. Mol Biol Evol. 2002; 19:640–653. [PubMed: 11961098]

Olson KA, Schell JC, Rutter J. Pyruvate and Metabolic Flexibility: Illuminating a Path Toward Selective Cancer Therapies. Trends Biochem Sci. 2016; 41:219–230. [PubMed: 26873641]

Pan M, Reid MA, Lowman XH, Kulkarni RP, Tran TQ, Liu X, Yang Y, Hernandez-Davies JE, Rosales KK, Li H, et al. Regional glutamine deficiency in tumours promotes dedifferentiation through inhibition of histone demethylation. Nat Cell Biol. 2016; 18:1090–1101. [PubMed: 27617932]

Pearce EL, Poffenberger MC, Chang CH, Jones RG. Fueling Immunity: Insights into Metabolism and Lymphocyte Function. Science. 2013; 342:1242454–1242454. [PubMed: 24115444]

Psychogios N, Hau DD, Peng J, Guo AC, Mandal R, Bouatra S, Sinelnikov I, Krishnamurthy R, Eisner R, Gautam B, et al. The human serum metabolome. PLoS ONE. 2011; 6:e16957. [PubMed: 21359215]

Reyes P, Guganig ME. Studies on a pyrimidine phosphoribosyltransferase from murine leukemia P1534J. Partial purification, substrate specificity, and evidence for its existence as a bifunctional complex with orotidine 5-phosphate decarboxylase. J Biol Chem. 1975; 250:5097–5108. [PubMed: 1171096]

Schug ZT, Peck B, Jones DT, Zhang Q, Grosskurth S, Alam IS, Goodwin LM, Smethurst E, Mason S, Blyth K, et al. Acetyl-CoA Synthetase 2 Promotes Acetate Utilization and Maintains Cancer Cell Growth under Metabolic Stress. Cancer Cell. 2015; 27:57–71. [PubMed: 25584894]

Schwartz PM, Handschumacher RE. Selective antagonism of 5-fluorouracil cytotoxicity by 4-hydroxypyrazolopyrimidine (allopurinol) in vitro. Cancer Res. 1979; 39:3095–3101. [PubMed: 455294]

Sellers K, Fox MP, Bousamra M II, Slone SP, Higashi RM, Miller DM, Wang Y, Yan J, Yuneva MO, Deshpande R, et al. Pyruvate carboxylase is critical for non–small-cell lung cancer proliferation. J Clin Invest. 2015; 125:687–698. [PubMed: 25607840]

Shaul YD, Yuan B, Thiru P, Nutter-Upham A, McCallum S, Lanzkron C, Bell GW, Sabatini DM. MERAV: a tool for comparing gene expression across human tissues and cell types. Nucleic Acids Res. 2016; 44:D560–D566. [PubMed: 26626150]

Smith CA, O'Maille G, Want EJ, Qin C, Trauger SA, Brandon TR, Custodio DE, Abagyan R, Siuzdak G. METLIN: a metabolite mass spectral database. Ther Drug Monit. 2005; 27:747–751. [PubMed: 16404815]

Smith LH Jr, Sullivan M, Huguley CM Jr. Pyrimidine Metabolism In Man. IV. The Enzymatic Defect of Orotic Aciduria. J Clin Invest. 1961; 40:656–664. [PubMed: 16695858]

Suchi M, Mizuno H, Kawai Y, Tsuboi T, Sumi S, Okajima K, Hodgson ME, Ogawa H, Wada Y. Molecular cloning of the human UMP synthase gene and characterization of point mutations in two hereditary orotic aciduria families. Am J Hum Genet. 1997; 60:525–539. [PubMed: 9042911]

Taguchi R, Ishikawa M. Precise and global identification of phospholipid molecular species by an Orbitrap mass spectrometer and automated search engine Lipid Search. J Chromatogr A. 2010; 1217:4229–4239. [PubMed: 20452604]

Tardito S, Oudin A, Ahmed SU, Fack F, Keunen O, Zheng L, Miletic H, Sakariassen PØ, Weinstock A, Wagner A, et al. Glutamine synthetase activity fuels nucleotide biosynthesis and supports growth of glutamine-restricted glioblastoma. Nat Cell Biol. 2015; 17:1556–1568. [PubMed: 26595383]

Traut TW, Jones ME. Kinetic and conformational studies of the orotate phosphoribosyltransferase:orotidine-5′-phosphate decarboxylase enzyme complex from mouse Ehrlich ascites cells. J Biol Chem. 1977; 252:8374–8381.

Vander Heiden MG, Cantley LC, Thompson CB. Understanding the Warburg Effect: The Metabolic Requirements of Cell Proliferation. Science. 2009; 324:1029–1033. [PubMed: 19460998]

Venneti S, Dunphy MP, Zhang H, Pitter KL, Zanzonico P, Campos C, Carlin SD, La Rocca G, Lyashchenko S, Ploessl K, et al. Glutamine-based PET imaging facilitates enhanced metabolic evaluation of gliomas in vivo. Sci Transl Med. 2015; 7:274ra17.

Wishart DS, Jewison T, Guo AC, Wilson M, Knox C, Liu Y, Djoumbou Y, Mandal R, Aziat F, Dong E, et al. HMDB 3.0--The Human Metabolome Database in 2013. Nucleic Acids Res. 2013; 41:D801–D807. [PubMed: 23161693]

Wu XW, Lee CC, Muzny DM, Caskey CT. Urate oxidase: primary structure and evolutionary implications. Proc Natl Acad Sci U S A. 1989; 86:9412–9416. [PubMed: 2594778]

Wu XW, Muzny DM, Lee CC, Caskey CT. Two independent mutational events in the loss of urate oxidase during hominoid evolution. J Mol Evol. 1992; 34:78–84. [PubMed: 1556746]

Wu X, Wakamiya M, Vaishnav S, Geske R, Montgomery C Jr, Jones P, Bradley A, Caskey CT. Hyperuricemia and urate nephropathy in urate oxidase-deficient mice. Proc Natl Acad Sci U S A. 1994; 91:742–746. [PubMed: 8290593]

Yamada T, Uchikata T, Sakamoto S, Yokoi Y, Fukusaki E, Bamba T. Development of a lipid profiling system using reverse-phase liquid chromatography coupled to high-resolution mass spectrometry with rapid polarity switching and an automated lipid identification software. J Chromatogr A. 2013; 1292:211–218. [PubMed: 23411146]

Yao C-H, Fowle-Grider R, Mahieu NG, Liu G-Y, Chen Y-J, Wang R, Singh M, Potter GS, Gross RW, Schaefer J, et al. Exogenous Fatty Acids Are the Preferred Source of Membrane Lipids in Proliferating Fibroblasts. Cell Chem Biol. 2016; 23:483–493. [PubMed: 27049668]

Yuneva MO, Fan TWM, Allen TD, Higashi RM, Ferraris DV, Tsukamoto T, Matés JM, Alonso FJ, Wang C, Seo Y, et al. The Metabolic Profile of Tumors Depends on Both the Responsible Genetic Lesion and Tissue Type. Cell Metab. 2012; 15:157–170. [PubMed: 22326218]

Zhang Y, Evans GB, Clinch K, Crump DR, Harris LD, Frohlich RFG, Tyler PC, Hazleton KZ, Cassera MB, Schramm VL. Transition State Analogues of Plasmodium falciparum and Human Orotate Phosphoribosyltransferases. J Biol Chem. 2013; 288:34746–34754. [PubMed: 24158442]

Highlights

- Systematic development of human plasma-like medium (HPLM)
- Culture in HPLM has widespread effects on cellular metabolism
- Culture in HPLM reveals uric acid as an endogenous inhibitor of UMPS
- Uric acid can influence cellular sensitivity to 5-fluorouracil

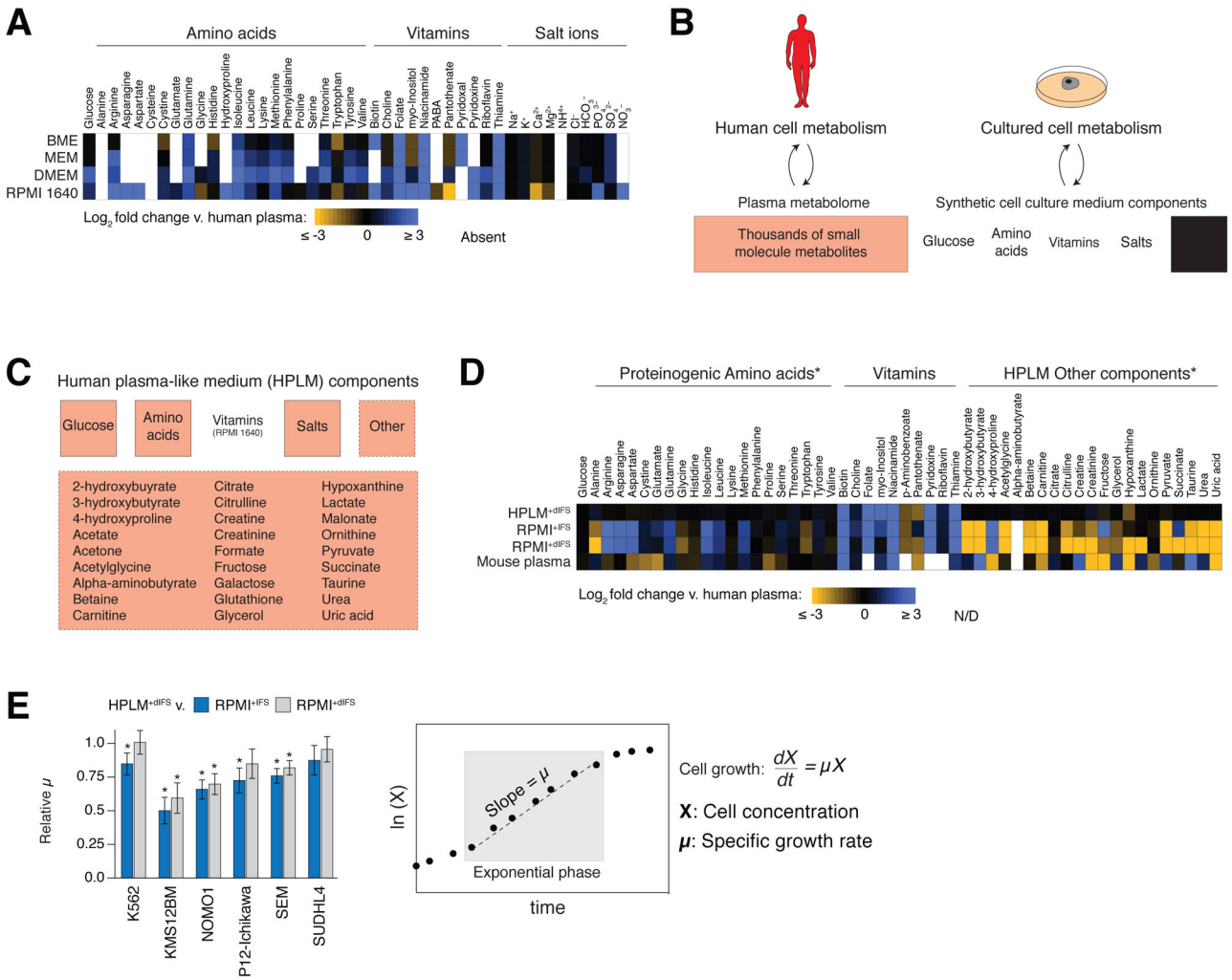

Figure 1. Figure 1, see also Figure S1 and Table S1: A cell culture medium that reflects the polar metabolite composition of human plasma

(A) Heatmap of relative concentrations of the indicated components of BME, MEM, DMEM, and RPMI 1640 compared to those in adult human plasma (log_2-transformed fold changes). Components not present in a medium are marked as absent. See Table S1 for further detail regarding this heatmap and the concentrations of all metabolites.

(B) Schematic depicting the different metabolic milieus to which cells in culture and *in vivo* are exposed.

(C) Components of human plasma-like medium (HPLM). The concentrations of the components depicted by red-colored boxes reflect those in adult human plasma. See Table S1 for the detailed formulation of HPLM.

(D) Heatmap of relative concentrations of the indicated components in denoted media and mouse plasma compared to those in human plasma (log_2-transformed fold changes). N/D, fold change value could not be determined. See Table S1 for detailed criteria used to generate this heatmap and for the concentrations of all metabolites. $RPMI^{+IFS}$: RPMI 1640 with 5 mM glucose and 10% IFS. $RPMI^{+dIFS}$: RPMI 1640 with 5 mM glucose and 10% dialyzed IFS. $HPLM^{+dIFS}$: HPLM containing 10% dialyzed IFS. *The following metabolites

were not readily detected in media samples by the metabolite profiling method used: acetate, acetone, cysteine, formate, galactose, glutathione, and malonate.

(E) Relative growth rates of six hematological cancer cell lines cultured in $HPLM^{+dIFS}$ compared to in $RPMI^{+IFS}$ (blue) or in $RPMI^{+dIFS}$ (gray) (mean ± SD, n = 3; *p < 0.05) (left). Specific growth rates (μ) were calculated using natural log-transformed growth curves (right). Cell lines represent the following hematological cancers: K562 (chronic myeloid leukemia), KMS12BM (multiple myeloma), NOMO1 (acute myeloid leukemia), P12-Ichikawa (T-cell acute lymphoblastic leukemia), SEM (B-cell acute lymphoblastic leukemia), SUDHL4 (B-cell lymphoma).

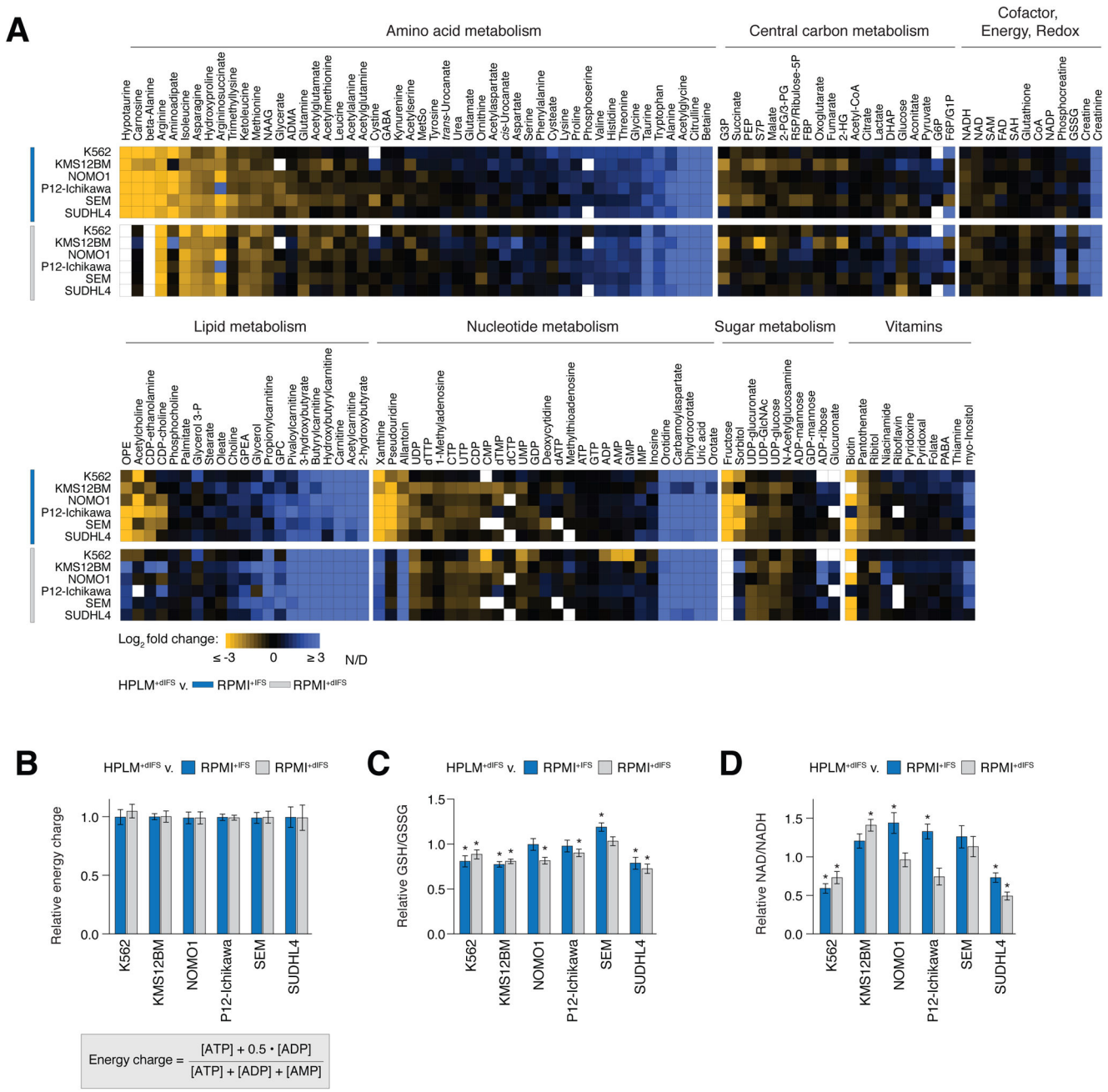

Figure 2. Figure 2, see also Figure S2 and Table S2: Culture of cells in HPLM extensively alters their metabolic landscape

(A) Heatmap of relative intracellular metabolite concentrations following culture in $HPLM^{+dIFS}$ compared to that in $RPMI^{+IFS}$ (top six rows) or to $RPMI^{+dIFS}$ (bottom six rows). Within each group, metabolites are sorted by average log_2-transformed fold change of the top six rows (n = 3). N/D, fold change value could not be determined because the metabolite was not readily detected following culture in one or more of the media. To be included in the heatmap, metabolites had to have a fold change measured in at least four of

the six cell lines. See Table S2 for detailed criteria used to generate this heatmap, metabolite abbreviations, and the concentrations of all metabolites.

(B) Energy charge values, as calculated by the displayed equation, following culture in $HPLM^{+dIFS}$ compared to that in $RPMI^{+IFS}$ (blue) or to $RPMI^{+dIFS}$ (gray) (mean ± SD, n = 3).

(C) Intracellular GSH/GSSG ratios following culture in $HPLM^{+dIFS}$ compared to that in $RPMI^{+IFS}$ (blue) or to $RPMI^{+dIFS}$ (gray) (mean ± SD, n = 3, *$p < 0.05$).

(D) Intracellular NAD/NADH ratios following culture in $HPLM^{+dIFS}$ compared to that in $RPMI^{+IFS}$ (blue) or to $RPMI^{+dIFS}$ (gray) (mean ± SEM, n = 3, *$p < 0.05$).

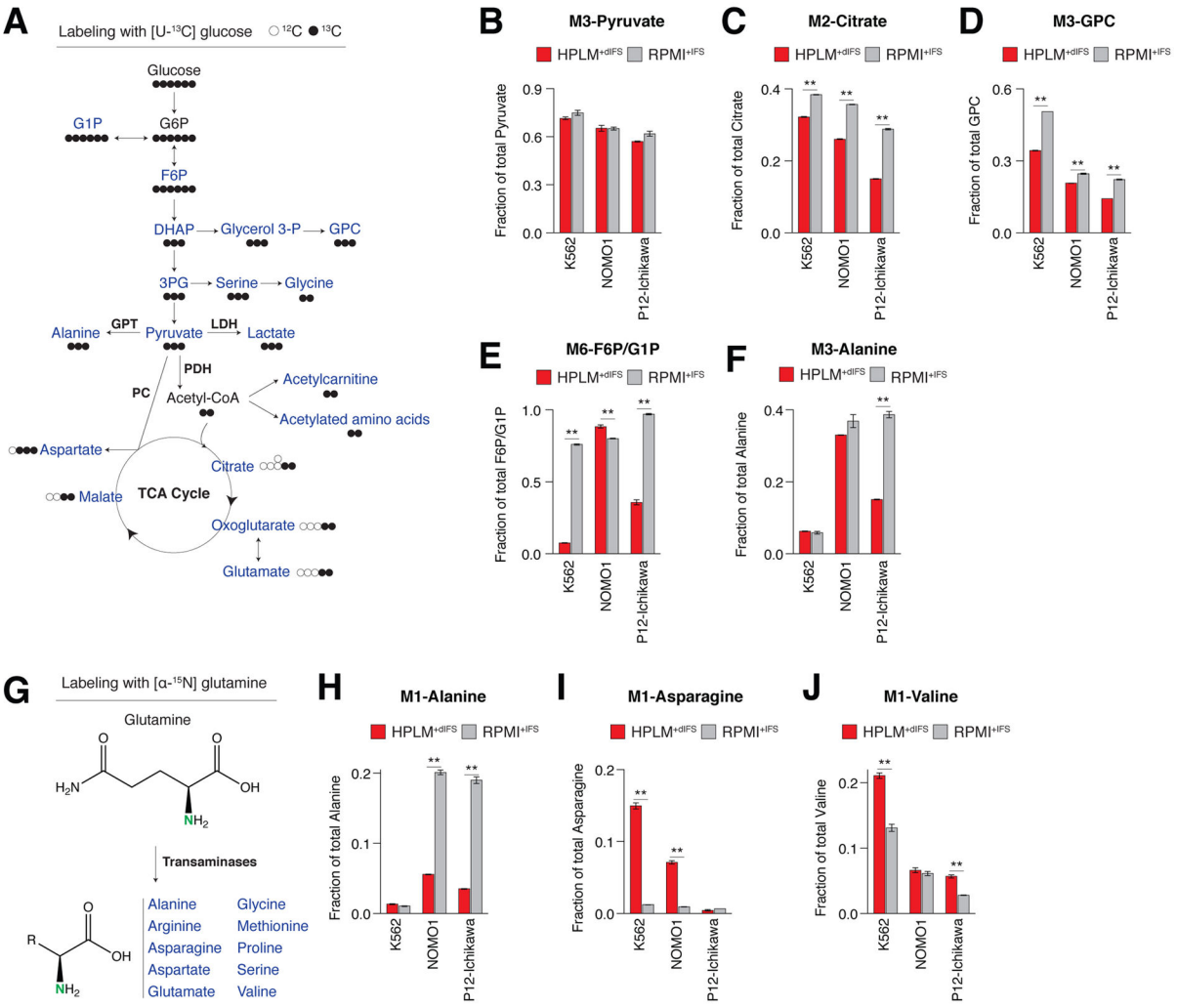

Figure 3. Figure 3, see also Figure S3 and Table S2: Culture of cells in HPLM^{+dIFS} affects the utilization of glucose carbons and the α-amino nitrogen of glutamine

(A) Schematic depicting the incorporation of ^{13}C from glucose into pathways branching from glycolysis and into pyruvate, and various fates of glucose-derived carbon from pyruvate and Acetyl-CoA, including into the TCA cycle. See Table S2 for ^{13}C labeling patterns for metabolites in blue. G1P: glucose 1-phosphate. G6P: glucose 6-phosphate. F6P: fructose 6-phosphate. DHAP: dihydroxyacetone phosphate. GPC: glycerophosphocholine. PDH: pyruvate dehydrogenase. LDH: lactate dehydrogenase. GPT: alanine aminotransferase.

(B) Fraction of pyruvate labeled with three ^{13}C (M3) following culture of cells in HPLM^{+dIFS} (red) or RPMI^{+IFS} (gray) (mean ± SD, n = 3).

(C) Fraction of citrate labeled with two ^{13}C (M2) following culture of cells in HPLM^{+dIFS} (red) or RPMI^{+IFS} (gray) (mean ± SD, n = 3; **p < 0.0005).

(D) Fraction of GPC labeled with three ^{13}C (M3) following culture of cells in HPLM^{+dIFS} (red) or RPMI^{+IFS} (gray) (mean ± SD, n = 3; **p < 0.0005).

(E) Fraction of F6P/G1P labeled with six ^{13}C (M6) following culture of cells in HPLM^{+dIFS} (red) or RPMI^{+IFS} (gray) (mean ± SD, n = 3; **p < 0.0005).

(F) Fraction of alanine labeled with three ^{13}C (M3) following culture of cells in $HPLM^{+dIFS}$ (red) or $RPMI^{+IFS}$ (gray) (mean ± SD, n = 3; **p < 0.0005).
(G) Schematic depicting the transaminase-mediate transfer of ^{15}N from the α-amino nitrogen of glutamine onto various amino acids. See Table S2 for ^{15}N labeling patterns for amino acids in blue.
(H) Fraction of alanine labeled with one ^{15}N (M1) following culture of cells in $HPLM^{+dIFS}$ (red) or $RPMI^{+IFS}$ (gray) (mean ± SD, n = 3; **p < 0.0005).
(I) Fraction of asparagine labeled with one ^{15}N (M1) following culture of cells in $HPLM^{+dIFS}$ (red) or $RPMI^{+IFS}$ (gray) (mean ± SD, n = 3; **p < 0.0005).
(J) Fraction of valine labeled with one ^{15}N (M1) following culture of cells in $HPLM^{+dIFS}$ (red) or $RPMI^{+IFS}$ (gray) (mean ± SD, n = 3; **p < 0.0005).

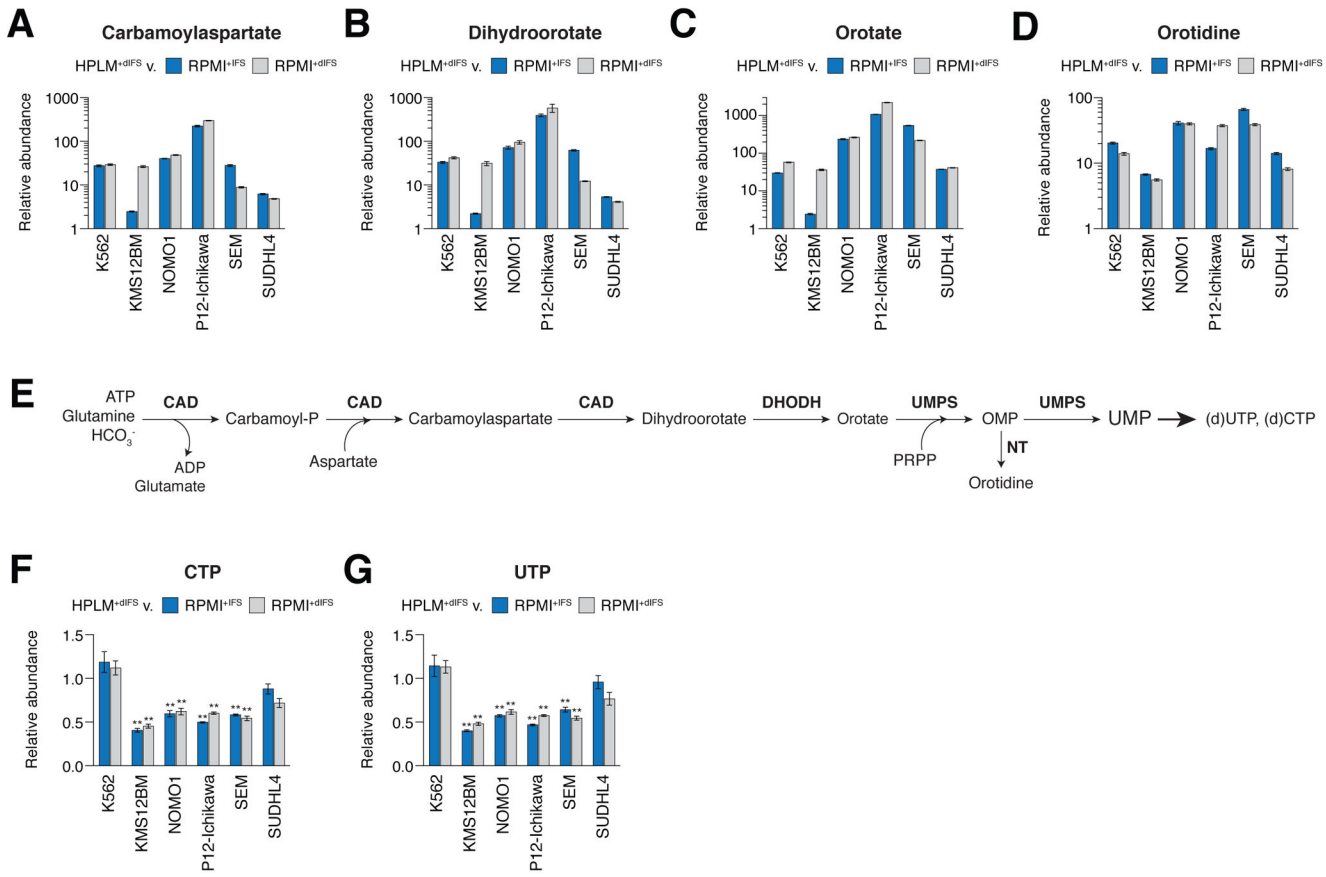

Figure 4. Figure 4, see also Figure S4: Culture in HPLM^{+dIFS} greatly affects the intracellular abundances of metabolites involved in pyrimidine metabolism

(A–D) Relative intracellular abundances of carbamoylaspartate (A), dihydroorotate (B), orotate (C), and orotidine (D) following culture of cells in HPLM^{+dIFS} compared to that in RPMI^{+IFS} (blue) or RPMI^{+dIFS} (red) (mean ± SD, n = 3; $p < 0.0005$ for all bars).

(E) Schematic depicting the de novo pyrimidine synthesis pathway. NT: nucleotidase.

(F and G) Relative intracellular abundances of CTP (F) and UTP (G) following culture of cells in HPLM^{+dIFS} compared to that in RPMI^{+IFS} (blue) or RPMI^{+dIFS} (gray) (mean ± SD, n = 3, **$p < 0.0005$).

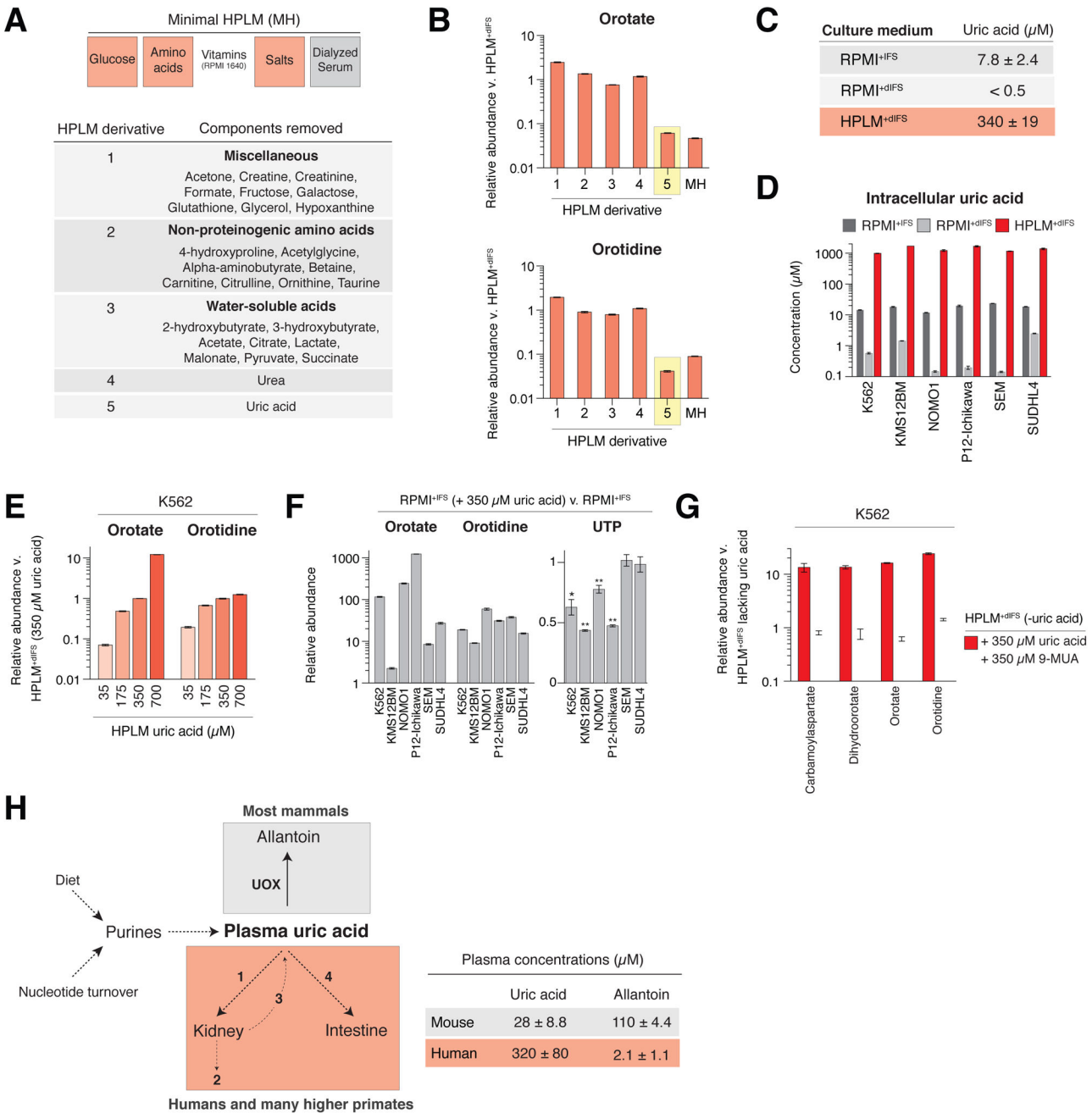

Figure 5. The uric acid component of HPLM^{+dIFS} mediates the effects of HPLM^{+dIFS} on pyrimidine metabolism

(A) Composition of minimal HPLM (top) and list of components removed from HPLM^{+dIFS} to generate the indicated dropout formulations (bottom).

(B) Relative intracellular abundances of orotate (top) and orotidine (bottom) following culture of cells in each HPLM^{+dIFS} derivative or minimal HPLM (MH) compared to that in complete HPLM^{+dIFS} (mean ± SD, n = 3). The number designations of the HPLM^{+dIFS} derivatives correspond to those in panel A.

(C) Concentrations of uric acid in RPMI^{+IFS} and HPLM^{+dIFS} as measured by LC/MS-based metabolite profiling (n = 4). Uric acid could not be readily detected in RPMI^{+dIFS} by the metabolite profiling method used. Thus, the indicated concentration for RPMI^{+dIFS} approximately corresponds to that of minimum detection in media samples.
(D) Intracellular concentrations of uric acid following culture of cells in RPMI^{+IFS}, RPMI^{+dIFS}, or HPLM^{+dIFS} (mean ± SD, n = 3).
(E) Relative intracellular abundances of orotate and orotidine following culture of K562 cells in HPLM^{+dIFS} containing increasing concentrations of uric acid compared to that in standard HPLM^{+dIFS}, which contains 350 μM uric acid (mean ± SD, n = 3).
(F) Relative intracellular abundances of orotate, orotidine (left) (mean ± SD, n = 3; $p < 0.0005$ for all bars), and UTP (mean ± SD, n = 3; *$p < 0.005$; **$p < 0.0005$) (right) following culture of cells in RPMI^{+IFS} supplemented with 350 μM uric acid compared to that in RPMI^{+IFS}.
(G) Relative intracellular abundances of carbamoylaspartate, dihydroorotate, orotate, and orotidine following culture of K562 cells in HPLM^{+dIFS} containing either 350 μM uric acid (red) or 350 μM uric acid 9-methyluric acid (9-MUA) (white) compared to that in HPLM^{+dIFS} lacking uric acid (mean ± SD, n = 3).
(H) Schematic depicting the pathways that influence the plasma concentrations of uric acid; 1: glomerular filtration (70%), 2: secretion (10%), 3: reabsorption (90%), 4: excretion (30%) (Bobulescu and Moe, 2012). In contrast to most mammals, humans and many higher primates lack uricase (UOX) activity, which converts uric acid to allantoin (left). Concentrations of uric acid and allantoin in mouse plasma as measured by metabolite profiling in this study (n = 4). Average concentration of uric acid in human plasma calculated from annotated values in the Human Metabolome Database. Concentration of allantoin in human plasma as reported elsewhere (Kand'ár and Záková, 2008) (right).

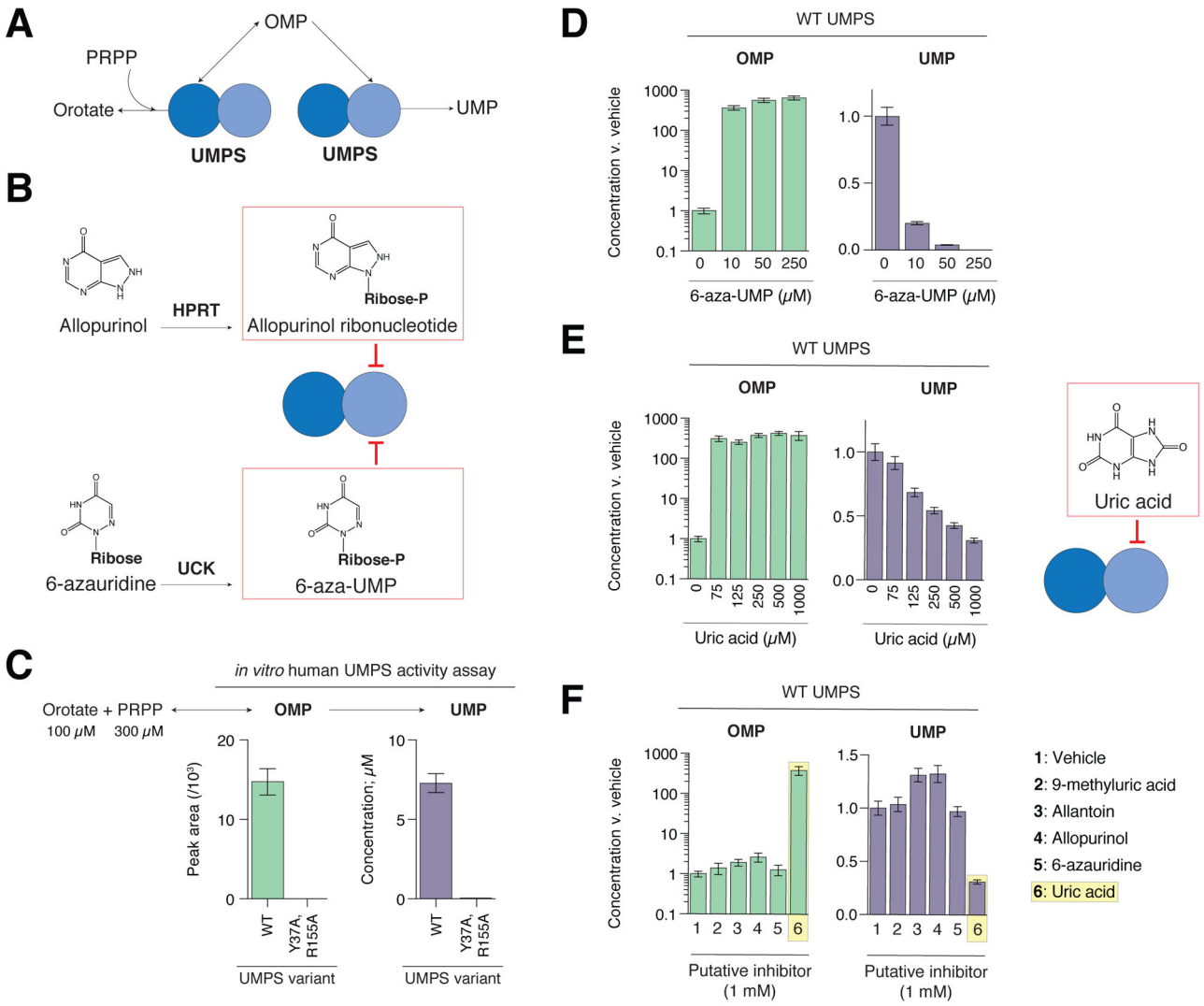

Figure 6. Figure 6, see also Figures S5 and S6: Uric acid is a direct inhibitor of UMPS

(A) Schematic depicting the reactions catalyzed by each domain of bifunctional UMP synthase (UMPS). OPRT: orotate phosphoribosyltransferase. ODC: OMP decarboxylase.

(B) Schematic depicting competitive inhibition of the ODC domain of UMPS by allopurinol ribonucleotide (top) and 6-aza-UMP (bottom). Hypoxanthine-guanine phosphoribosyltransferase (HPRT) catalyzes the conversion of allopurinol to its ribonucleotide derivative, and uridine-cytidine kinase (UCK) catalyzes that of 6-azauridine to 6-aza-UMP.

(C) Quantification of OMP (left) and UMP (right) following incubation of recombinant UMPS (WT or the Y37A, R155A mutant) with its substrates orotate and PRPP at the indicated concentrations (mean ± SD, n = 3). WT: wild-type.

(D) Relative abundances of OMP (left) and UMP (right) following addition of increasing concentrations of 6-aza-UMP or vehicle to the UMPS activity assay (mean ± SD, n = 3).

(E) Relative abundances of OMP (left) and UMP (middle) following addition of increasing concentrations of uric acid or vehicle to the UMPS activity assay (mean ± SD, n = 3).

Schematic depicting competitive inhibition of the ODC domain of UMPS by uric acid (right).

(F) Relative abundances of OMP (left) and UMP (right) following addition of 9-methyluric acid, allantoin, allopurinol, 6-azauridine, uric acid, or vehicle to the UMPS activity assay (mean ± SD, n = 3).

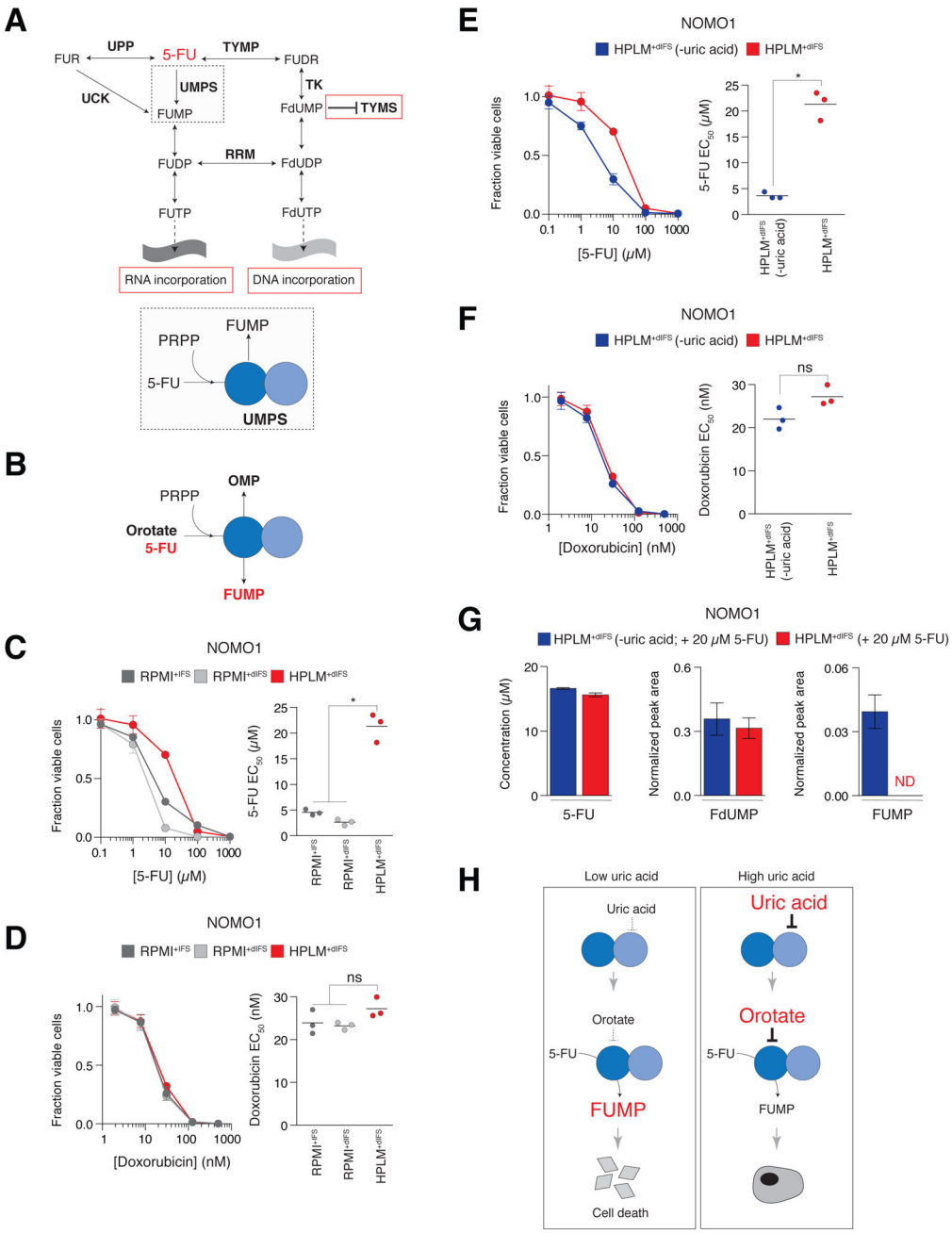

Figure 7. Figure 7, see also Figure S7: Uric acid antagonizes the cytotoxicity of 5-fluorouracil

(A) Schematic depicting the metabolism of 5-fluorouracil (5-FU) (top). 5-FU is converted into various fluoronucleotide derivatives that mediate its cytotoxic effects. Fluorouridine triphosphate (FUTP) and fluorodeoxyuridine triphosphate lead to cell death upon misincorporation into RNA and DNA, respectively. Fluorodeoxyuridine monophosphate (FdUMP) leads to cell death by inhibition of thymidylate synthase (TYMS) (Longley et al., 2003). Enzymes depicted are uridine phosphorylase (UPP), uridine-cytidine kinase (UCK), thymidine phosphorylase (TYMP), thymidine kinase (TK), and ribonucleotide reductase (RRM). Other metabolites indicated are fluorouridine (FUR), fluorouridine monophosphate

(FUMP), fluorouridine diphosphate (FUDP), fluorodeoxyuridine (FUDR), and fluorodeoxyuridine diphosphate (FdUDP). The OPRT domain of UMPS catalyzes the direct conversion of 5-FU to FUMP (bottom).

(B) Schematic showing that the OPRT domain of UMPS catalyzes the conversions of orotate to OMP and 5-FU to FUMP.

(C and D) Dose-response of NOMO1 cells to 5-FU (C) or doxorubicin (D) when cultured in $RPMI^{+IFS}$ (dark gray), $RPMI^{+dIFS}$ (light gray), or $HPLM^{+dIFS}$ (red) (mean ± SD, n = 9). Data points are the average of three independent biological experiments that each consisted of three technical replicates (left). EC_{50} of 5-FU (C) or doxorubicin (D) in NOMO1 cells when cultured in $RPMI^{+IFS}$ (dark gray), $RPMI^{+dIFS}$ (light gray), or $HPLM^{+dIFS}$ (red). Horizontal bar indicates the mean of three independent biological experiments; * $p < 0.001$; ns: not significant (right).

(E and F) Dose-response of NOMO1 cells to 5-FU (E) or doxorubicin (F) when cultured in $HPLM^{+dIFS}$ (green) or $HPLM^{+dIFS}$ lacking uric acid (blue) (mean ± SD, n = 9). Data points are the average of three independent biological experiments that each consisted of three technical replicates (left). EC_{50} of 5-FU (C) or doxorubicin (D) in NOMO1 cells when cultured in $HPLM^{+dIFS}$ (red) or $HPLM^{+dIFS}$ lacking uric acid (blue). Horizontal bar indicates the mean of three independent biological experiments; * $p < 0.001$; ns: not significant (right).

(G) Intracellular abundances of 5-FU (left), FdUMP (middle), and FUMP (right) in NOMO1 cells treated with 20 μM 5-FU and cultured for 24 hr in $HPLM^{+dIFS}$ (red) or $HPLM^{+dIFS}$ lacking uric acid (blue) (mean ± SD, n = 3). ND: not detected.

(H) Proposed mechanism of uric acid-mediated antagonism of cytotoxicity caused by 5-FU. As either the OPRT domain of UMPS or the sequential actions of UPP and UCK can convert 5-FU to FUMP, the influence of uric acid on 5-FU sensitivity likely depends on the extent that a given cell type generates FUMP via OPRT-mediated synthesis.